A modeling study on the climate impacts of black carbon aerosols

Chien Wang

Massachusetts Institute of Technology, Cambridge, Massachusetts, USA

Received 18 August 2003; revised 25 November 2003; accepted 8 December 2003; published 6 February 2004.

[1] A three-dimensional interactive aerosol-climate model has been developed and used to study the climatic impact of black carbon (BC) aerosols. When compared with the model's natural variability, significant global-scale changes caused by BC aerosols occurred in surface latent and sensible heat flux, surface net long-wave radiative flux, planetary boundary layer height, convective precipitation (all negative), and low-cloud coverage (positive), all closely related to the hydrological cycle. The most significant regional change caused by BC revealed in this study is in precipitation that occurs in the tropics (shift of precipitation center in the ITCZ) and in the middle and high latitudes of the Northern Hemisphere (change in snow depth). Influenced by BC caused changes in cloud cover and surface albedo, the interactive model provides smaller positive all-sky forcing at the top of atmosphere (TOA) and larger negative forcing at the surface than the offline diagnostics (the direct forcings). The actual solar radiative forcings by BC derived from the interactive model also exhibit significant interannual variations that are up to 4 times as large as their means. Based on the revealed changes in cloud radiative forcing by BC, a non-Twomey-Albrecht indirect forcing by BC that alters radiative budgets by changing cloud cover via thermodynamics rather than microphysics is also defined. It has been demonstrated that with an absolute amount more than 2 times higher than that of the TOA forcing, the surface forcing by BC is a very important factor in analyzing the climatic impact of BC. The result of this study suggests that with a constant annual emission of 14 TgC, BC aerosols do not cause a significant change in global-mean surface temperature. The calculated surface temperature change is determined by a subtle balance among changes in surface energy budget as well as in the hydrological cycle, all caused by BC forcing and often compensate each other. The result of this study shows that the influences of BC aerosols on climate and environment are more significant in regional scale than in global scale. Important feedbacks between BC radiative effects and climate dynamics revealed in this study suggest the importance of using interactive aerosol-climate models to address the issues related to the climate impacts of aerosols. *INDEX TERMS:* 0305 Atmospheric Composition and Structure: Aerosols and particles (0345, 4801); 0345 Atmospheric Composition and Structure: Pollution—urban and regional (0305); 1620 Global Change: Climate dynamics (3309); 3337 Meteorology and Atmospheric Dynamics: Numerical modeling and data assimilation; 3319 Meteorology and Atmospheric Dynamics: General circulation; *KEYWORDS:* black carbon, aerosols, climate change

Citation: Wang, C. (2004), A modeling study on the climate impacts of black carbon aerosols, *J. Geophys. Res.*, *109*, D03106, doi:10.1029/2003JD004084.

1. Introduction

[2] Direct radiative forcing by black carbon (BC) aerosols at the top of atmosphere (TOA) has been calculated in various studies and the estimated values range from $\sim$+0.16 to +0.80 W/m^2, depending on the treatment of their mixing states [e.g., *Haywood and Shine*, 1995; *Haywood et al.*, 1997; *Haywood and Ramaswamy*, 1998; *Penner et al.*, 1998; *Myhre et al.*, 1998; *Cooke et al.*, 1999; *Tegen et al.*, 2000; *Jacobson*, 2001; *Koch*, 2001; *Chung and Seinfeld*, 2002]. This forcing represents a considerable amount of heating of the atmosphere and has been conjectured as a potential factor causing global warming [e.g., *Hansen et al.*, 1998; *Jacobson*, 2001]. However, strong extinction of solar radiation by means of both scattering and absorbing effects of BC leads to a reduction of incoming solar radiation at the Earth's surface, as revealed by observations [e.g., *Satheesh and Ramanathan*, 2000; *Ramanathan et al.*, 2001a, 2001b] or suggested by theoretical studies [e.g., *Hansen et al.*, 1998; *Haywood and Ramaswamy*, 1998; *Chung et al.*, 2002], and hence, like sulfate aerosols, introduces a cooling effect at the surface.

[3] It is obvious that the changes in surface energy budget caused by the direct forcing of aerosols can be quite complicated. The balance between altered surface radiative

0148-0227/04/2003JD004084$09.00

and heat fluxes caused by aerosols determines the actual impact of aerosols on surface temperature changes. Previous modeling studies suggest that at current time, the cooling caused by sulfate aerosols represents a significant offset in value to the warming effect caused by so-called greenhouse gases such as CO_2, CH_4, N_2O, and O_3 [*Roeckner et al.*, 1999; *Ramaswamy et al.*, 2001]. In the case of BC aerosols, however, the uneven heating/cooling effect across the Earth's surface further complicates the surface energy budget and thus the otherwise near constant relationship between the radiative forcing of a given species and the resultant change in surface temperature established for other radiatively important species [e.g., *Manabe and Wetherald*, 1967].

[4] Interestingly enough, these BC aerosol induced changes in radiative or heat fluxes and resultant changes in temperature can potentially perturb clouds and precipitation as well as atmospheric circulation and thus eventually impact on the physical effect of BC's radiative forcing as well as BC's lifetime in the troposphere. This is because that when a given BC layer coexists with a cloud layer, whether this BC layer is located below or above the cloud layer critically determines the actual radiative effects of these aerosols. In addition, the atmospheric abundance of BC is primarily influenced by precipitation [e.g., *Liousse et al.*, 1996; *Cooke et al.*, 1999; *Cooke et al.*, 2002], while the atmospheric distributions of BC is largely determined by circulation. It is clear that the above-mentioned processes can form a two-way feedback mechanism between radiative forcings of BC aerosols and climate dynamics that is essential in determining the climate impact of these aerosols. The close interaction between BC aerosols and climate suggests the importance of using an interactive aerosol-climate model, a model including the transient two-way feedback mechanism between BC aerosols and climate dynamics as well as physics, to investigate the climate impact of aerosols. Unfortunately, due to its complexity, such analyses are still rare for BC aerosols.

[5] This article presents a study using a three-dimensional interactive aerosol-climate system model developed based on the Climate System Model (CSM) of the National Center for Atmospheric Research (NCAR) [see *Boville and Gent*, 1998; *Kiehl et al.*, 1998] to explore the climate impact of BC as an additional component to atmospheric aerosols. The model description is given first in the paper, followed by the discussions on the modeled results including radiative forcings of BC aerosols as well as their influences on climate dynamics and physics. The principal conclusions are then summarized.

2. Model Description

[6] Black carbon aerosols are treated as externally mixed aerosols in a single mode with a given size spectral function in this model [e.g., *Wilson et al.*, 2001]. Like the majority of current BC models summarized by *Penner et al.* [2001], a single-moment scheme that uses mass mixing ratio as the only prognostic variable to describe the atmospheric evolution of BC aerosols is used. The atmospheric transport of aerosols is calculated by the same procedure as other tracers such as water vapor in the NCAR Community Climate Model version 3 (CCM3) [see *Kiehl et al.*, 1996; *Kiehl et al.*, 1998] at each time step. Dry deposition and gravitational sedimentation of aerosols are included. The bulk dry deposition speed of BC aerosols is given to be 0.1 cm/s, adopted from several previous studies [e.g., *Cooke and Wilson*, 1996; *Liousse et al.*, 1996]. The gravitational sedimentation speed is given as the dry deposition speed multiplied by an approximated pressure correction factor of $(p_{00}/p)^{0.286}$ [*Twomey*, 1977a; *Wang and Chang*, 1993], here p_{00} and p are the sea level air pressure and the air pressure at a given vertical layer, respectively. Wet scavenging of aerosols in the model includes removal processes of aerosols by liquid droplets and by ice particles based on the impact scavenging calculation [*Wang and Chang*, 1993; *Wang and Prinn*, 2000], with an approximate collection coefficient of 0.01 for liquid droplets and 0.005 for ice particles [*Pruppacher and Klett*, 1997]. The nucleation scavenging of BC aerosols are not included [e.g., *Flossmann et al.*, 1985]. The scavenging rate at a given grid point of the model is thus derived as:

$$\frac{1}{q_a}\frac{dq_a}{dt} = -C\left(p_{00}\Big/p\right)^{0.286} q_p. \tag{1}$$

Here q_a and q_p are the mass mixing ratios of BC aerosols and precipitation particles in kg/kg, respectively; dt has a unit of seconds. For the liquid precipitation scavenging where the temperature is above freezing point, the value of C (in kg kg^{-1} s^{-1}) is 4.51×10^{-2} for convective clouds and 5.18×10^{-2} for stratiform clouds. The value of C for ice particle scavenging (assumed to happen when temperature is below freezing point) is calculated based on snowflakes [*Wang and Chang*, 1993] and appears to be quite close to the C value for stratiform clouds multiplied by 0.5 (i.e., 2.59×10^{-2}). To simplify the coding in program, this value is thus used for the ice particle scavenging calculation. In the model calculation, q_p at a given vertical layer is actually an accumulation from the cloud top to this layer with reduction by evaporation considered or the total precipitation passed the given vertical layer between two adjacent wet scavenging calculations (2400 s for the T42 run). Precipitation particles have a good chance to fall through the clouds during this time period. Note that q_a is defined at each model grid. Using this scheme, the tropospheric lifetime of BC aerosols yielded is about 4.6 days, very close to the result of *Liousse et al.* [1996] (4–4.5 days), *Cooke et al.* [1999] (5.8 days), *Cooke et al.* [2002] (4.3 days), and *Koch* [2001] (4.3–4.4 days) while appears to be shorter than that obtained in *Cooke and Wilson* [1996] for a fossil-fuel-only calculation (7.85 days). Obviously, implementing microphysical processes in a GCM with several hundreds kilometer resolution is a "dangerous" work. This issue will be further addressed by ongoing studies, incorporating surface property transitions of aerosols due to chemical reactions and microphysics in a high-resolution model with comprehensive physics and chemistry, to derive parameterizations for GCMs and to assess the uncertainty of this type of approximations.

[7] The inclusion of BC aerosols in the 18-band solar radiation module of CCM3 [*Briegleb*, 1992] is formulated following *Kiehl and Briegleb* [1993], and three sets of optical parameters of BC aerosols are derived based on previous works using the Mie scattering theory to investi-

Table 1. Optical Parameters of BC Aerosols for the Waveband 0.35–0.64 μm Used in the Model

	Specific Extinction Coefficient, m^2/g	Single Scattering Albedo	Asymmetry Factor
Model 1	7.93	0.26	0.75
Model 2	12.50	0.25	0.42
Model 3	15.37	0.40	0.42

gate the influence of different size spectra or scattering calculations on the climate impact of BC. The first set of parameters is derived based on *Jennings and Pinnick* [1980], *Twitty and Weinman* [1971], and *Liousse et al.* [1996]. The second set is adopted from *Haywood and Shine* [1995], where a lognormal size distribution is applied. The third set is derived based on a revised gamma distribution [e.g., *Twitty and Weinman*, 1971] and a scheme for spherical particles described by *Bohren and Huffman* [1983]. The values of these parameters for the 0.35–0.64 μm waveband are listed in Table 1. Hereinafter, model runs using these parameter sets are referred to as Models 1, 2, and 3, respectively. The surface albedo in the model is calculated interactively by the NCAR Land Surface Model (LSM) [see *Bonan*, 1998] coupled with the CCM3. By including the aerosol radiative effects into prognostic procedures in the CCM3 radiation module, the aerosols are allowed to interact with climate dynamics when that option is being chosen.

[8] The emissions of BC from both fossil fuel and biomass burning are used in this study (Figure 1). The fossil fuel emissions of BC are derived based on (1) the energy use for coal, gas, and oil specified in the MIT Emissions and Policy Prediction Analysis Model (EPPA) [see *Prinn et al.*, 1999; *Babiker et al.*, 2001]; (2) consumption of refined petroleum products from International Energy Agency (IEA) (available at http://www.iea.org); and (3) BC and OC emission coefficients for different fuel types (coal, refined oil, and gas) and different sources from *Cooke et al.* [1999]. The biomass burning emissions of BC are derived based on *Crutzen and Andreae* [1990] and *Liousse et al.* [1996]. The emissions are mapped onto a $1° \times 1°$ global grid first. Depending on the source of the emissions, a population density map [*Li*, 1996] for emissions from fossil fuel combustion and biomass burning in households or the land use maps [*Olivier et al.*, 1995] for biomass burning other than the households kind are employed. Details in deriving these emissions are described by *Mayer et al.* [2000]. Then the emissions data for different model resolutions are derived based on this $1° \times 1°$ dataset. The annual BC emission used in this study is ~14 TgC, partitioned as ~8 TgC from fossil fuel burning and ~6 TgC from biomass burning. The BC annual emissions are kept constant through the model integrations to emphasize the study on feedbacks between BC radiative forcings and climate dynamics.

[9] In this study, comparison of two groups of different model runs, one (REF) which excludes and the other (BCRAD) which includes the radiative effect of BC as well as associated influences on climate dynamics, isolates the climate effect of BC (note that both types of runs predict atmospheric evolution of BC). To further isolate this effect, instead of a dynamically changed one a constant "background" sulfate aerosol field is used in the model, which comes with the CCM3 distribution. Note although this is consistent with the external mixing assumption made in this study, the possible influence of this setup on the modeled

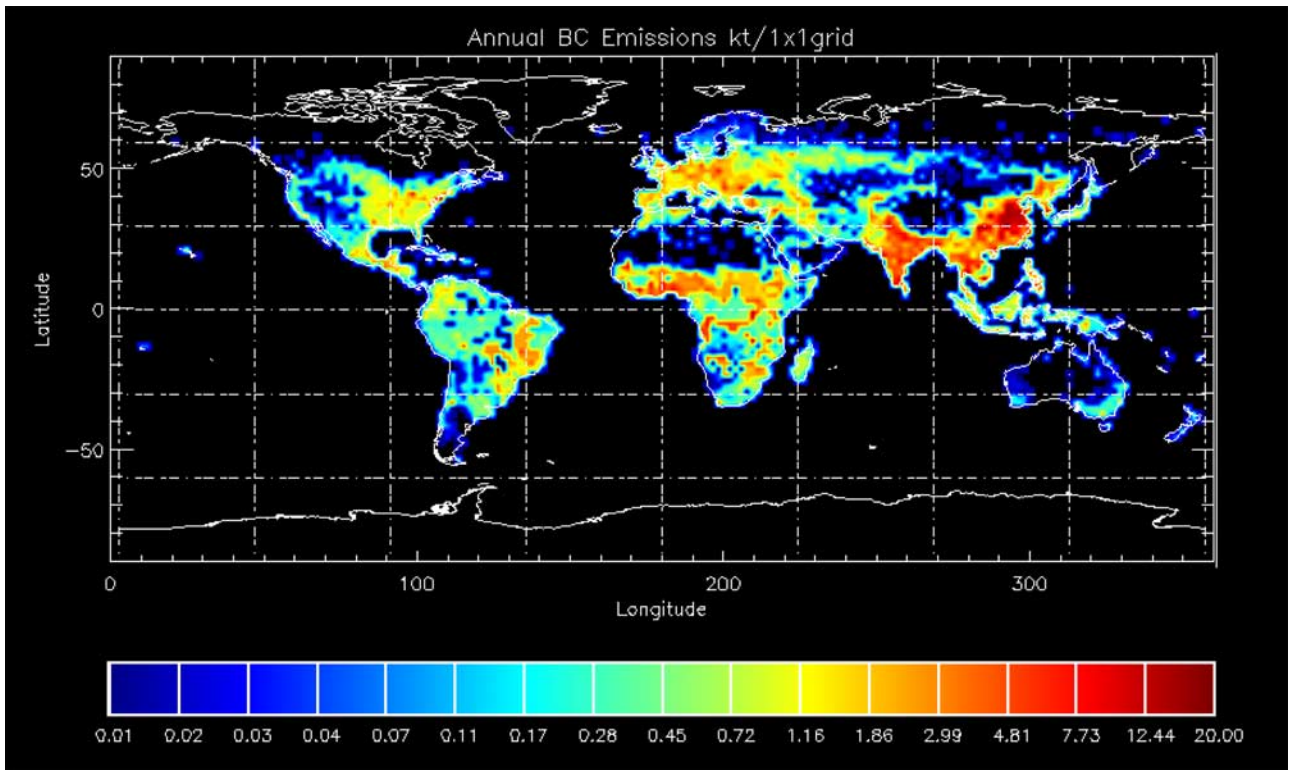

Figure 1. Annual emissions of black carbon aerosols used in the study. The unit is GgC per $1° \times 1°$ grid.

Table 2. Brief Description of Model Runs in This Study[a]

Symbol of Run	Interactive BC	Ocean	BC Optical Parameters
SOM REF	No	SOM	(Note)[b]
SOM BCRAD	Yes	SOM	Model 1
OSST REF	No	OSST	(Note)[b]
OSST BCRAD (Model 1)	Yes	OSST	Model 1
OSST BCRAD (Model 2)	Yes	OSST	Model 2
OSST BCRAD (Model 3)	Yes	OSST	Model 3
CSST REF	No	CSST	(Note)[b]
CSST BCRAD (Model 1)	Yes	CSST	Model 1
CSST BCRAD (Model 2)	Yes	CSST	Model 2
CSST BCRAD (Model 3)	Yes	CSST	Model 3

[a]SOM = slab ocean model; OSST = observed SST; CSST = climatological SST; REF = runs excluding BC radiative effect; and BCRAD = runs including BC radiative effect.

[b]Note: Each reference run calculates all three types of diagnostic radiative forcings of BC with corresponding optical parameters.

results might need to be assessed when a more comprehensive model, which includes internal mixtures of aerosols, becomes available. The term of "changes caused by BC" used in the later discussions is referred to the differences between the results of BCRAD and REF runs. The direct radiative forcings of BC aerosols in REF runs using different optical parameter sets of BC, which are in line with the International Panel on Climate Control (IPCC) [*Houghton et al.*, 1996] definition of aerosol's direct radiative forcing, have also been derived for comparison purpose without being actually used in the model (the two-way aerosol-climate interaction is excluded in the REF runs). These diagnostically derived forcings will be referred as offline forcings hereafter. Note that by repeating diagnostic radiation calculation several times, each REF run can derive all three types of offline forcings with corresponding optical parameter set.

[10] To shorten the required computing time of the model runs, the full three-dimensional ocean general circulation model in the CSM model family is not incorporated with the atmospheric model (CCM3) and the land surface model (LSM) that are both used in this study. In stead, three types of model runs are carried out. In the first type of runs (OSST runs), the sea surface temperatures (SSTs) are prescribed using an analyzed observational monthly SST dataset (available at http://www.cgd.ucar.edu/cms/ccm3) that covers the time period from 1978 to 1998 (240 months in total). In order to evaluate the impact of prescribed SST data on the OSST run results during a specific time period, the second type of model runs has also been launched that repeats a 12-month climatological SST data 20 times (CSST runs). In the third type of runs, a slab ocean model distributed with the CCM3.6.6 with a simple ice model [*Kiehl et al.*, 1996] has been used (SOM runs). With these different model settings, there are 10 model runs in total, three REF runs as well as seven BCRAD runs that use different optical parameters of BC (Table 2). Note that by neglecting the oceanic feedback to BC forcings, the runs with prescribed SST (OSST and CSST runs) represent the lower bound of the model response to BC forcings. On the other hand, the slab ocean model is a simplified mixed layer ocean model that calculates the mixed layer temperature based on the atmospheric heat fluxes at the ocean's surface and parameterized ocean transport as well as heat exchanges between the mixed layer and deep ocean. Therefore with a limited heat capacity of the ocean, SOM runs perhaps represent the upper limit of the system response to BC forcings. The model runs with prescribed SST are mainly used to reveal short-term interannual variability and relationships among given parameters. The SOM model runs are mainly designed to study the equilibrium climate effects of BC. Comparisons among various model runs reveal the role of oceanic response in BC-climate interaction. The model 1 OSST and SOM results will be emphasized in discussions to reduce the size of the paper unless indicated otherwise.

[11] The horizontal resolution of the model used in this study is $2.8^\circ \times 2.8^\circ$ (T42). There are 18 vertical layers from the Earth's surface to $\sim$3 hPa. The integration times of OSST and CSST runs are 20 years to consider the influence of model variability on the results. The integration times of SOM runs are 60 years; the last 20 years of the results are used to provide the equilibrium status of climate under the forcings of BC aerosols. The entire model integrations were processed on a 32-node PC cluster at MIT.

[12] In order to provide a measure of the statistical significance or the signal/noise ratio for the changes caused by BC aerosols, standard deviations of various model variables based on their annual means over the entire integration period, both as quantities at each model grid point (functions of latitude and longitude) and as global means, are calculated from the REF runs. The procedure is to calculate the annual means of these quantities first and then to derive the standard deviation of the integration period using corresponding annual means. These standard deviations represent the "natural variability" of the model during the integration period. They will be referred to later in the paper as the "reference standard deviations (σ_r)" to be distinguished with the standard deviations of changes of various parameters caused by BC aerosols. Note that when mentioned in the later part of the paper, this "natural variability of the model" is only applied to the given model integration period.

[13] The modeled highest atmospheric loading of BC appears in the East Asia, primarily the east part of China, and the Indian subcontinent (Figure 2a). Other areas with high loading of BC aerosols include eastern and central United States, Europe, central Africa, and Brazil. Interestingly, model results clearly indicate two transport pathways of BC aerosols, one from the East Asia to North America and the other from Europe to northern polar regions. These modeled characteristics of BC spatial distributions are

Figure 2. (a) Model simulated vertical column loading of BC aerosols (in g/km^2; top panel), (b) aerosol index derived from satellite observations (middle panel), and (c) model simulated zonal mean distribution of BC aerosol concentration (in ng/kg; bottom panel). All model results are 20-year means based on the OSST BCRAD run. The monthly POLDER satellite AI data kindly provided by F.-M. Bréon and S. Generoso cover a time period from November 1996 to June 1997. These data are averaged over time and then interpolated into the T42 grid ($2.8^\circ \times 2.8^\circ$) used in the model.

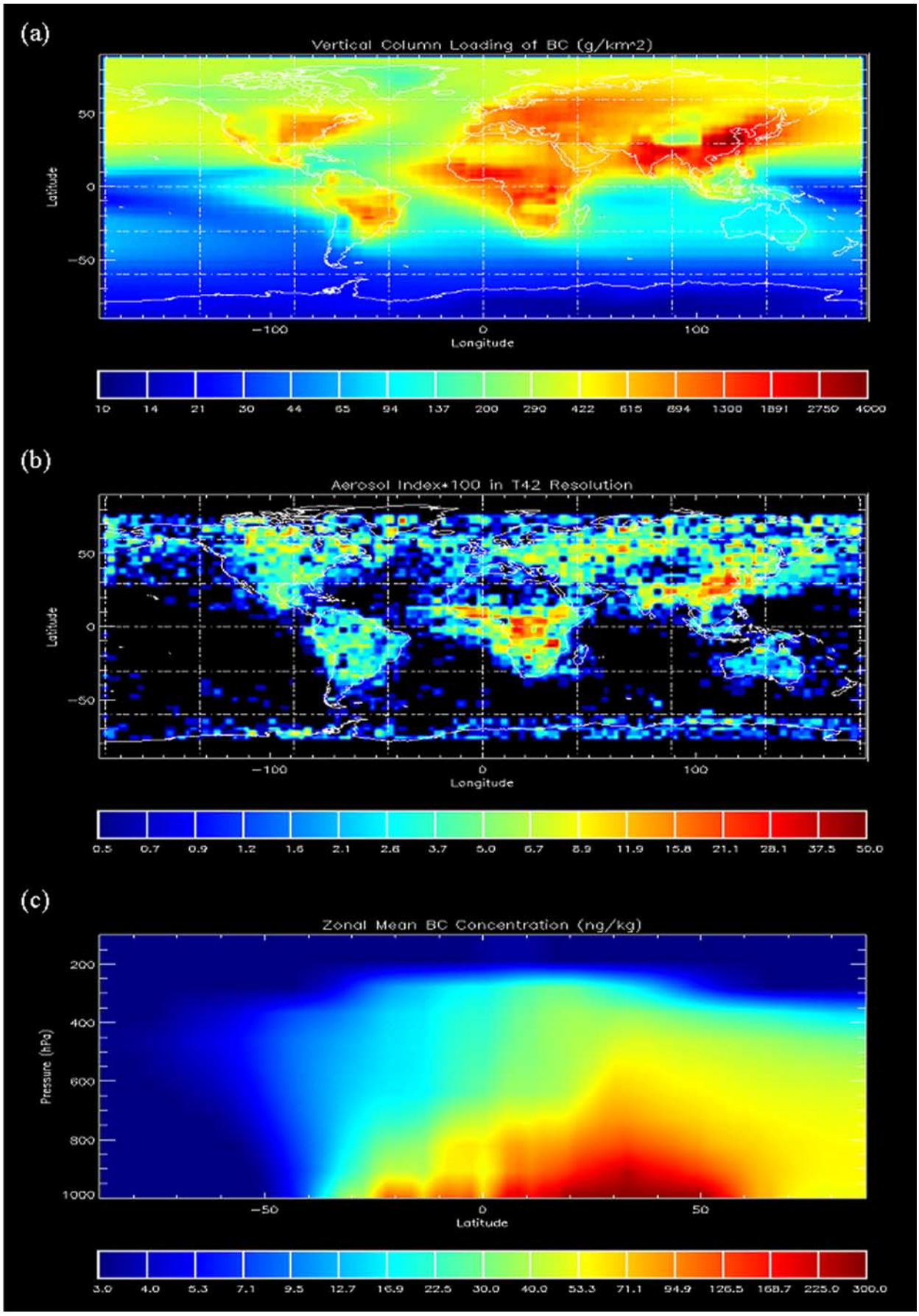
(a)
Vertical Column Loading of BC (g/km^2)
Latitude
50
0
−50
−100
0
100
Longitude
10 14 21 30 44 65 94 137 200 290 422 615 894 1300 1891 2750 4000
(b)
Aerosol Index*100 in T42 Resolution
Latitude
50
0
−50
−100
0
100
Longitude
0.5 0.7 0.9 1.2 1.6 2.1 2.8 3.7 5.0 6.7 8.9 11.9 15.8 21.1 28.1 37.5 50.0
(c)
Zonal Mean BC Concentration (ng/kg)
Pressure (hPa)
200
400
600
800
1000
−50
0
50
Latitude
3.0 4.0 5.3 7.1 9.5 12.7 16.9 22.5 30.0 40.0 53.3 71.1 94.9 126.5 168.7 225.0 300.0

Figure 2.

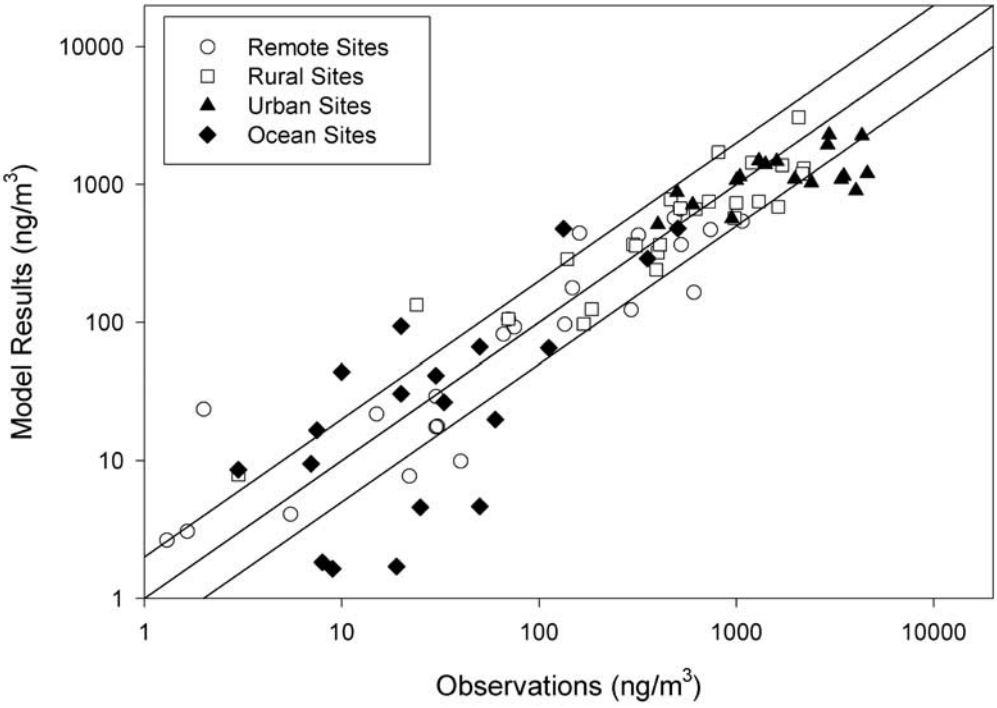

Figure 3. Comparison between observed and modeled surface BC concentrations at a number of locations. Observational data are from *Liousse et al.* [1996] and *Cooke et al.* [1999]. The unit of BC concentration is ng/m^3.

well supported by the satellite observational data of small particles with biomass or human pollution origins, i.e., the "aerosol index" (AI) derived from the measurements of the POLDER instruments onboard the ADEOS satellite shown in Figure 2b [*Bréon et al.*, 2002]. A good correlation between modeled column loading or surface concentrations of BC and satellite AI data, especially for the land regions where the high AI is located, is also found in comparisons between these two parameters point by point over the model grid resolution (i.e., T42; not shown). Although the lifetime of black carbon aerosols in the atmosphere is rather short (~5 days in this model), it can be longer in the upper troposphere. Model results indicate that in the middle and upper troposphere a considerable amount of BC aerosols that originated from Europe and East Asia have been transported toward higher altitudes (Figure 2c) and over the northern oceans (Figures 2a and 2c). The appearances of BC aerosols in these high latitude areas are relatively persistent due to lower wet scavenging rate as compared to the middle and low latitudes.

[14] In addition to the comparison with satellite data, the modeled surface BC concentrations have been compared with (somewhat limited) surface observations including point data summarized by *Liousse et al.* [1996] and *Cooke et al.* [1999] (Figure 3) and several station data (Figure 4). The agreement between modeled surface concentrations and the point data is generally within a factor of 2 except for some oceanic or remote sites as well as highly polluted urban sites, comparable to nine other models reviewed by *Penner et al.* [2001]. It is worth noting that the model, primarily due to its coarse spatial resolution, tends to overestimate or underestimate BC concentrations at oceanic or remote sites with extremely low concentrations and underestimate at urban sites where very high concentrations of BC exist [see also *Cooke et al.*, 2002]. When compared with the station data, the modeled results generally agree well with the Barrow and Amsterdam Island measurements in both seasonal cycle and concentrations (note that constant emissions are used in this study). However, an overestimation in modeled Mauna Loa surface concentration along with a slight switch in seasonal cycle can be seen clearly in Figure 4c. Interestingly, a similar disagreement between modeled and observed results for the Mauna Loa station can be found in the work of *Cooke et al.* [1999] and *Cooke et al.* [2002]. Therefore this might suggest a necessary further adjustment in East Asia emissions [e.g., *Streets et al.*, 2001].

[15] The total BC atmospheric burden averaged over 20 years of the model integration period of OSST runs is about 0.17 TgC with interannual variations smaller than 2%. It appears to be smaller than the central value obtained in the IPCC model intercomparison (0.133 TgC from biomass burning +0.133 TgC from fossil fuel; note that simple addition might not be valid here due to nonlinear precipitation scavenging) [see *Penner et al.*, 2001]. However, it is still within the commonly estimated range (i.e., 0.15–0.25 TgC) [*Cooke et al.*, 1999; *Koch*, 2001; *Chung and Seinfeld*, 2002; *Cooke et al.*, 2002].

3. Solar Radiative Forcings Caused by Black Carbon

[16] Four types of changes in net downward solar radiative flux caused by BC, namely changes at the TOA and at surface, both for all sky (including clouds) and clear sky,

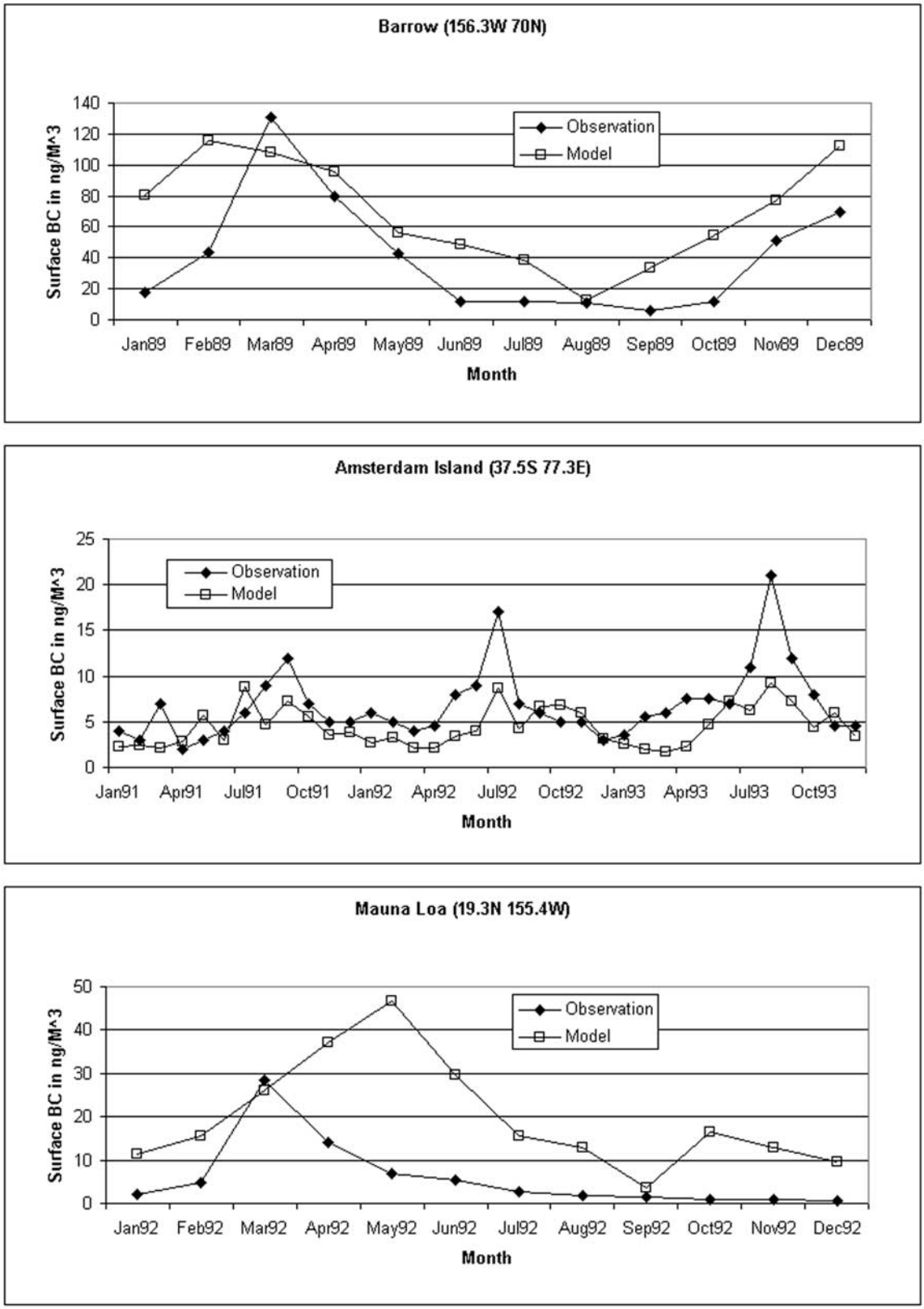

Figure 4. Comparison between modeled and observed surface concentrations of BC aerosols at three stations: (a) Barrow (top panel), (b) Amsterdam Island (middle panel), and (c) Mauna Loa (bottom panel). Observational data of Barrow and Mauna Loa site are from *Bodhaine* [1995]; the Amsterdam Island data are from *Liousse et al.* [1996].

have been derived by subtracting the results of the REF runs from those of the BCRAD runs:

$$\Delta F_{BC}(x,y,h,t) = \Delta F_{BCRAD}(x,y,h,t) - \Delta F_{REF}(x,y,h,t). \quad (2)$$

Here, x, y, and t are indices of longitude, latitude, and time, respectively; h represents either the TOA or the Earth's surface; ΔF_{BC} represents the change in net downward solar radiative flux caused by BC and hereafter is referred to as the "online forcing" or simply "forcing" for convenience and to distinguish it from the "offline forcing" described later; two ΔF terms on the right hand side of the equation are the net downward fluxes of solar radiation respectively in the BCRAD and REF runs. Note that the clear-sky fluxes are derived diagnostically in the CCM3 radiation code [*Briegleb*, 1992], mainly for the purpose to estimate the cloud forcing.

[17] As a comparison to the online radiative forcings of BC derived using equation (2) based on the interactive aerosol-climate model runs, the offline solar radiative forcings of BC aerosols are also derived from the REF runs using:

$$\Delta F_{BC}^{offline}(x,y,h,t) = \Delta F_{REFBC}(x,y,h,t) - \Delta F_{REF}(x,y,h,t). \quad (3)$$

Here ΔF_{REFBC} represents the diagnostic net downward flux of solar radiation if BC radiative effects were included (note that the REF runs predict the atmospheric distributions of BC aerosols but exclude BC's radiative effect in radiation calculation, therefore, these fluxes are derived only for diagnostic purpose and have not been actually used in the radiation calculation); ΔF_{REF} is the net downward flux derived by excluding BC from radiative calculation (the actual flux used in REF run); other variables have the same meanings as in equation (2).

[18] Note that the offline forcings derived from REF runs using equation (3) is in line with the definition of direct aerosol forcing of the IPCC [*Houghton et al.*, 1996]. The online forcings defined in equation (2), however, are different quantities than those IPCC defined ones. The online forcings are actual forcings to the atmosphere-surface system caused by BC when BC-climate interaction is included. These forcings represent the combinations of BC direct effect and several possible indirect effects as well as their feedbacks attributed to changes in BC loading, surface albedo, and cloud covers caused by the inclusion of BC direct radiative effect in the model.

3.1. Spatial Distribution of Direct BC Forcings

[19] The modeled offline clear-sky results indicate that the direct forcing by black carbon aerosols is primarily concentrated in the Northern Hemisphere with some clear extensions over the Southern Hemisphere (Figure 5). Contrasting with the positive atmospheric forcings (represented by the forcings at the TOA) are significant negative surface forcings located mainly over East Asia, South Asia, and Central Africa. When weighted by the natural variability of the model excluding BC, i.e., divided by the reference standard deviation, the direct TOA radiative forcings of BC (or the warming potential of the atmosphere) appear to be much more visible over waters near the major land emission sources than over the land, ranging from west Northern Atlantic and east tropical Atlantic, Mediterranean Sea, Arabian Sea, to the west edge of Pacific (Figure 6a). While at the surface, the weighted direct forcing by BC is very strong over the lands of major emission sources although the surface forcings of BC over the above-mentioned waters are also very significant (Figure 6b). The significant BC forcings over oceans in comparison with modeled natural variability, especially on the top of the atmosphere, suggest a potential influence of BC aerosols on ocean-atmosphere exchanges and thus on SST as well as oceanic air temperature.

3.2. Mean Features of Various BC Solar Forcings

[20] The global mean radiative forcings by BC appear to be positive at the TOA (warms the atmosphere) but negative at the Earth's surface (cools the ground). In addition, the magnitudes of the online all-sky forcing at surface are about triple those at the TOA. This ratio is nearly a constant throughout the whole integration period in various model runs. In OSST runs, the 20-year means of online BC solar forcing using model 1 are 0.27 and 0.22 W/m^2 at the TOA for clear sky and all sky and -0.57 and -0.64 W/m^2 at the surface for clear sky and all sky, respectively. The online TOA forcings of model 2 and 3 runs are quite close to the model 1 results, while the surface forcings differ slightly more (Table 3). In comparison, the online forcings derived from SOM runs are also close to the results of OSST runs, with a slightly stronger surface forcing than the OSST model result.

[21] Modeled result shows that the integration means of offline forcings are very close to the online ones in the clear-sky category (Table 4), suggesting the global and annual mean effect of the feedbacks via changes in BC loading and surface albedo to radiative forcings are rather small. In the all-sky category, although the offline forcings have the same signs as the online ones, they are much larger at the TOA but smaller at the surface than the online forcings in absolute values, implying that the perturbations caused by BC aerosols on cloud cover have significantly modified the radiative forcings of these aerosols. The offline forcings derived from SOM REF run are almost the same as those in OSST REF run (Table 4).

3.3. Interannual and Latitudinal Variations of BC Solar Forcings

[22] The online forcings (even as annual means) appear to have very large interannual variations, represented by their ranges and standard deviations (Figures 7a and 7b, Table 3). Interestingly, model runs with recycled SST (CSST runs) also showed the similar results so that the interannual variation of observed SST is not a major factor in causing the interannual variations of online forcings (Figures 7a and 7b). Opposite to the time evolution of online radiative forcings, the annual means of offline forcings vary little during the model integration period (Figures 7a and 7b, Table 4), indicating that the interannual variation of BC atmospheric burden is too small ($<\pm 2\%$ of total loading) to cause large perturbations in BC direct radiative forcings.

[23] The latitudinal distributions of online clear-sky forcings by BC derived from the last 20-year means of SOM runs are very close to those derived based on the 20-year means of OSST runs (Figure 7c) except for the sharp changes in SOM results around 60°S caused by

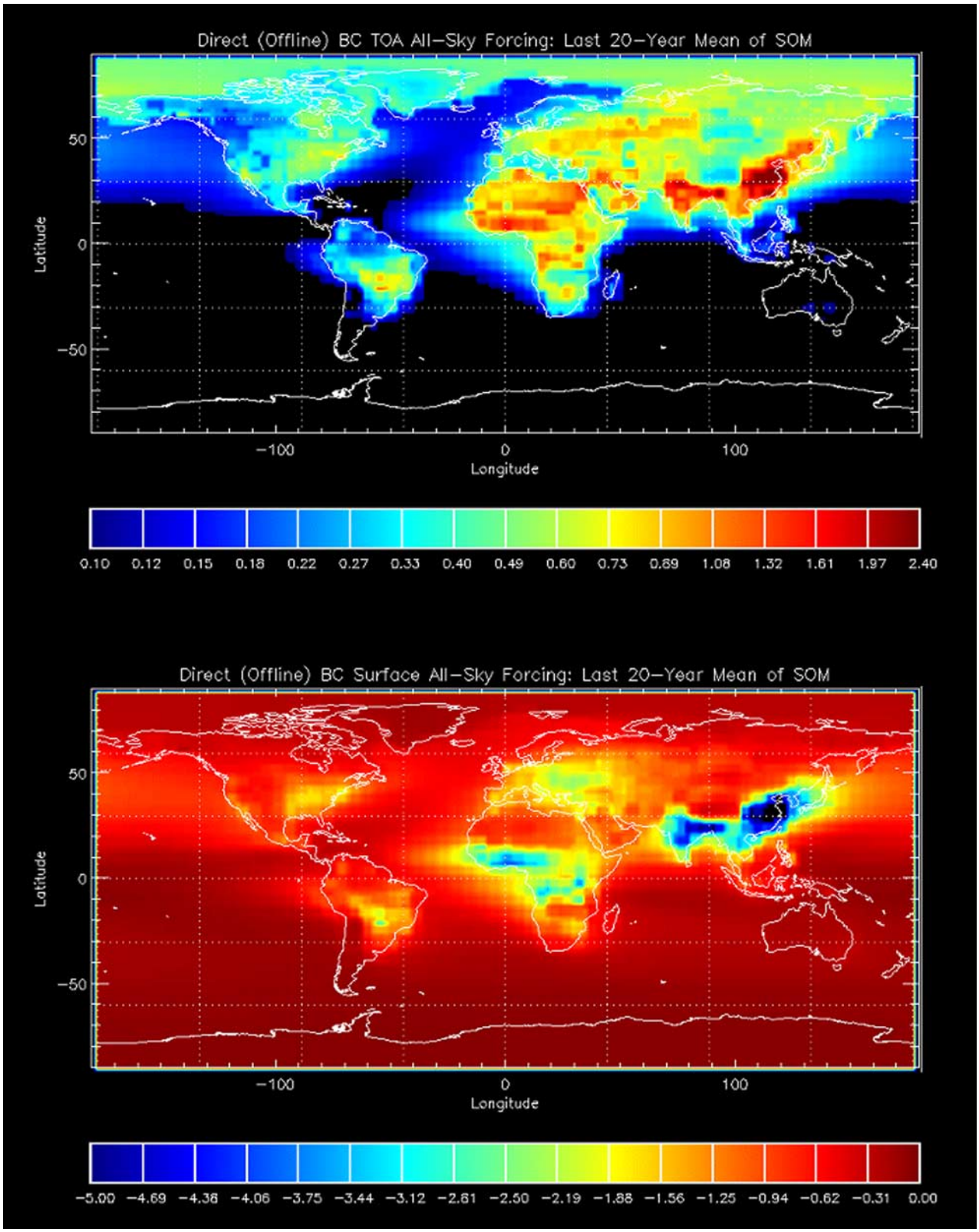

Figure 5. Modeled annual-mean direct (offline clear-sky) radiative forcings of BC (in W/m^2) at the top of atmosphere (upper panel) and the Earth's surface (lower panel). Results are derived from the last 20 years data of SOM REF run.

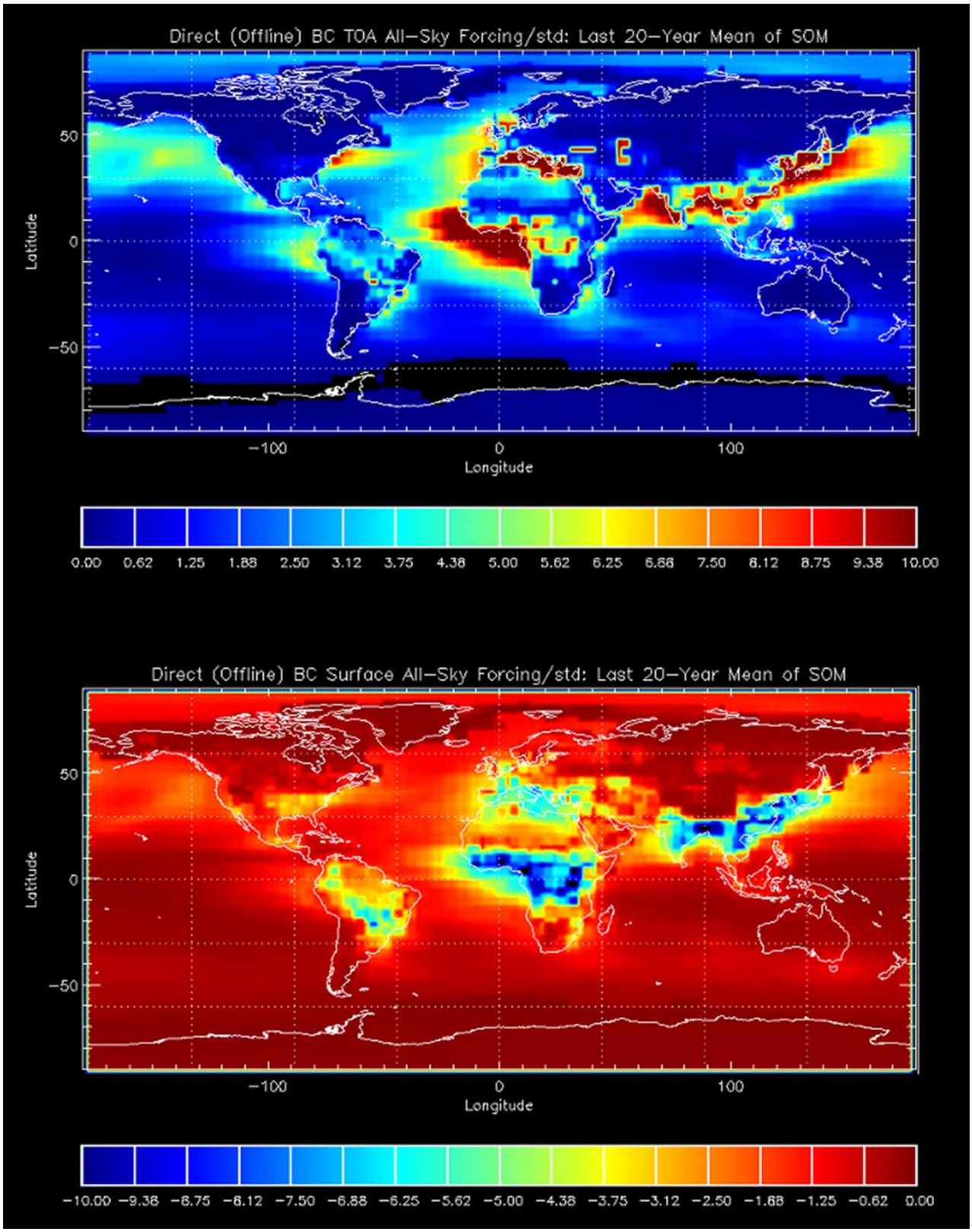

Figure 6. Same as Figure 5 except for ratios of modeled offline clear-sky BC forcings to the reference standard deviation at the top of the atmosphere (upper panel) and surface (lower panel).

Table 3. Annual and Global Means of Various Online Radiative Forcings of BC Presented as Integration Period Mean ± Standard Deviation (Range)[a]

	TOA Clear Sky	TOA All Sky	Surface Clear Sky	Surface All Sky
OSST Model 1	0.27 ± 0.08 (0.28)	0.22 ± 0.24 (0.85)	−0.57 ± 0.07 (0.24)	−0.64 ± 0.27 (0.99)
OSST Model 2	0.25 ± 0.08 (0.28)	0.22 ± 0.22 (0.89)	−0.60 ± 0.09 (0.36)	−0.64 ± 0.26 (1.09)
OSST Model 3	0.28 ± 0.06 (0.26)	0.20 ± 0.19 (0.76)	−0.80 ± 0.07 (0.30)	−0.92 ± 0.23 (0.91)
SOM	0.30 ± 0.10 (0.37)	0.14 ± 0.31 (1.17)	−0.63 ± 0.14 (0.50)	−0.80 ± 0.35 (1.39)

[a]All in W/m^2. The results of OSST runs are based on the annual means of 20 years; the results of SOM run are based on the annual means of the last 20 years.

the changes in sea ice that has very little effect on the global climate features. This suggests that the climatological spatial distributions of BC are almost the same in OSST and SOM model runs. On the contrary, although the online all-sky forcings predicted by SOM and OSST runs are in a good agreement over the high latitudes of the Northern Hemisphere as well as over most part of the Southern Hemisphere, their values sharply differ between 5°S and 60°N (Figure 7d), mainly induced by the difference in cloud cover between these two types of runs (see later discussions).

3.3.1. Cause of the Interannual Variations of BC Clear-Sky Forcing

[24] The model result shows that the magnitude of the difference in BC loadings between BCRAD and REF runs is small (a few percent of total BC loadings) and very close to that of the interannual variation of total BC loading (Figure 8). It has been found that in the zonal-mean base, the difference in clear-sky forcings between online and diagnostic offline results are negatively correlated to the BC loading changes between REF and BCRAD runs in most latitudes except for a few latitudinal bands in the middle and high latitudes of the Northern Hemisphere, where a positive correlation between the two parameters exists (not shown). The latter result suggests that the difference between online and offline radiative forcings over these midlatitude and high-latitude locations in the Northern Hemisphere must have been caused by a feedback between BC forcings and its resultant change in surface albedo.

[25] Indeed, detailed analysis has revealed that the interannual variation of online clear-sky solar forcing is primarily related to that of the surface albedo changes caused by BC forcing through altering surface snow depth, mainly in the middle and high latitudes of the Northern Hemisphere (Figures 9 and 10). Modeled results show that BC aerosols cause decreases in surface snow depth as large as 15 mm over a vast area of midlatitude and high-latitude lands and increases in the high latitude of North America, a part of Greenland, and several sites over the Eurasian continent, most related to relatively wet regions. BC aerosols can cause these changes in snow depth through several different processes, including atmospheric heating that causes clouds to dissipate or precipitation to decrease, and the reduction of solar radiation at the surface to preserve the snow layer. In addition, the adiabatic cooling or heating caused by BC in the boundary layer, depending on the vertical locations of aerosol layers [e.g., *Hansen et al.*, 1997], can impact on the formation and dissipation of low level clouds as well as the accumulation/evaporation of snow. The location appears to be important because the thermodynamic perturbation by BC is much more effective in low temperature. As shown in Figures 9 and 10, because the model predicted snow depth in most areas in the high latitudes of the Northern Hemisphere is equal to or lower than 100 mm except for Greenland, the change in snow depth caused by BC (quite often ±20%) produces a considerable change in surface albedo in these areas where the snow depth really matters. Note that there are some BC caused changes in snow depth in the Antarctic, however, these changes are very small in a relative meaning due to the large background value of snow depth (>300 mm) over Antarctica, the resultant effect on albedo hence is almost invisible.

3.3.2. Cause of the Interannual Variations of BC All-Sky Forcing

[26] Although the mean all-sky radiative forcings of BC averaged over the entire integration period are close to those of clear-sky ones as shown in Figures 7a and 7b and Table 3, the ranges of variation of all-sky forcings are more than 3 times as large as those of clear-sky forcings as indicated earlier. In particular, this large interannual variation occurred in all three sets of model runs (i.e., SOM, OSST, and CSST) and thus has little to do with the interannual fluctuations of SST. It has been found that the variations in all-sky forcings are closely related to the changes of cloud cover, in particular over the Northern Hemisphere and also in the tropics, induced by BC radiative forcing (Figure 11). In addition, the spatial distributions of all-sky forcings caused by BC (not shown) are more scattered compared with the clear-sky ones and spread out over both land and ocean. Strong connections between low-cloud cover change and BC

Table 4. Annual and Global Means of Various Offline Radiative Forcings of BC Presented as Integration Period Mean ± Standard Deviation (Range)[a]

	TOA Clear Sky	TOA All Sky	Surface Clear Sky	Surface All Sky
OSST Model 1	0.24 ± 0.00 (0.01)	0.34 ± 0.01 (0.02)	−0.57 ± 0.01 (0.02)	−0.47 ± 0.01 (0.03)
OSST Model 2	0.28 ± 0.00 (0.02)	0.42 ± 0.01 (0.02)	−0.73 ± 0.01 (0.04)	−0.61 ± 0.01 (0.04)
OSST Model 3	0.24 ± 0.00 (0.01)	0.39 ± 0.01 (0.02)	−0.78 ± 0.01 (0.05)	−0.64 ± 0.01 (0.04)
SOM Model 1	0.24 ± 0.00 (0.02)	0.35 ± 0.00 (0.02)	−0.59 ± 0.01 (0.04)	−0.48 ± 0.01 (0.03)
SOM Model 2	0.29 ± 0.00 (0.02)	0.43 ± 0.01 (0.02)	−0.75 ± 0.01 (0.05)	−0.63 ± 0.01 (0.04)
SOM Model 3	0.25 ± 0.01 (0.02)	0.40 ± 0.01 (0.02)	−0.80 ± 0.01 (0.05)	−0.66 ± 0.01 (0.04)

[a]All in W/m^2. The results of OSST runs are based on the annual means of 20 years; the results of SOM run are based on the annual means of 60 years.

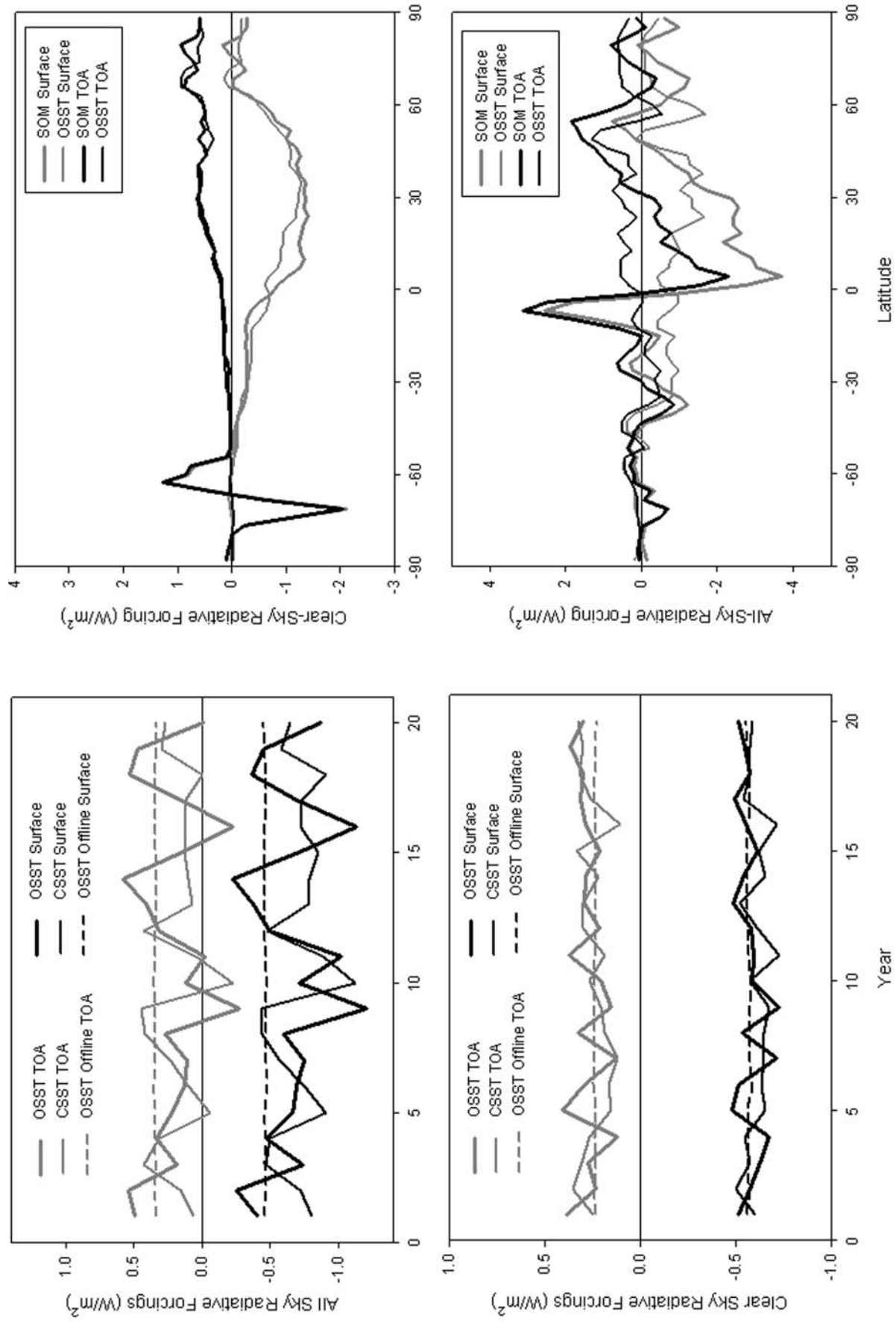
SOM Surface
OSST Surface
SOM TOA
OSST TOA
Clear-Sky Radiative Forcing (W/m²)
All-Sky Radiative Forcing (W/m²)
Latitude
OSST TOA
CSST TOA
OSST Offline TOA
OSST Surface
CSST Surface
OSST Offline Surface
All Sky Radiative Forcings (W/m²)
Clear Sky Radiative Forcings (W/m²)
Year

Figure 7.

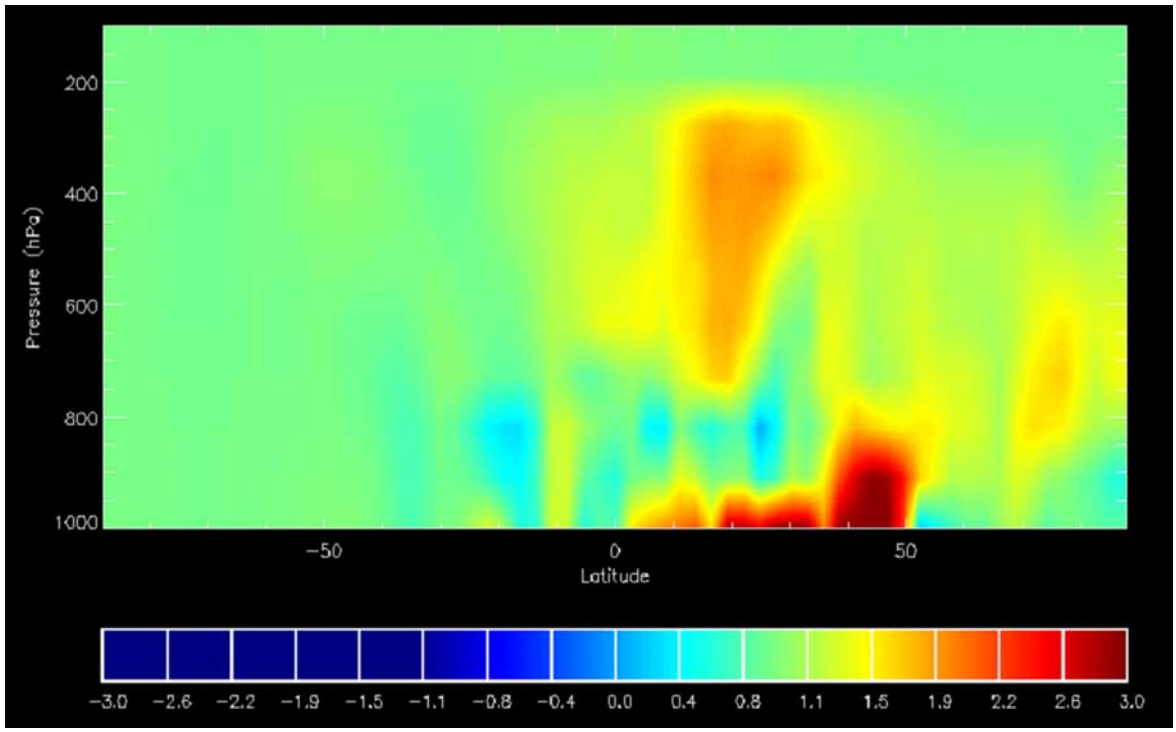

Figure 8. Modeled difference between BC mixing ratios in BCRAD and REF OSST runs in ng/kg. Results are derived as zonal means based on the 20-year averages of OSST runs.

TOA all-sky forcing in OSST and CSST runs and between convective clouds and BC all-sky forcings in SOM runs have also been identified. All these results indicate a modification of radiative forcing of clouds and thus suggest the possible existence of an ''indirect forcing'' by BC.

3.4. A Nonconventional Indirect Forcing of BC Aerosols

[27] The indirect forcing of aerosols traditionally refers to a process in which aerosols impact climate not by directly altering atmospheric radiation but by changing cloud properties and thus the radiative budget, through an increase of atmospheric concentrations of cloud condensation nuclei (CCN) that produces optically thicker and more reflecting clouds [*Twomey*, 1977b] or leads to a decrease of precipitation and hence an increase of abundance of certain clouds [*Albrecht*, 1989]. Besides these two mechanisms, absorbing aerosols such as BC may alter cloud properties through thermodynamic processes such as changing the vertical radiation or temperature profile and thus the atmospheric stability and circulation, or enhancing evaporation by warming the cloudy air to cause dissipation or partial dissipation of clouds. These processes have been discussed by *Ackerman et al.* [2000], *Lohmann and Feichter* [2001], *Chung et al.* [2002], as well as *Menon et al.* [2002], mostly under various specific conditions (more generic discussions can be also found in the work of *Haywood and Boucher* [2000] and *Ramanathan et al.* [2001a]). The radiative forcing formed through these above-discussed (mainly thermodynamic) processes should be called as a ''non-Twomey-Albrecht'' indirect forcing (NTAIF), or as suggested by *Hansen et al.* [1998], the ''semidirect'' forcing. Obviously, the indirect forcing caused by BC revealed in this study must be a NTAIF, since BC aerosols are not allowed to serve as CCNs in this model. This NTAIF can be defined as the difference between BC's all-sky solar forcing and its clear-sky solar forcing, or in other words, the cloud forcing change purely caused by BC aerosols:

$$NTAIF(x,y,h,t) = \Delta F_{BC}^{allsky}(x,y,h,t) - \Delta F_{BC}^{clearsky}(x,y,h,t) \quad (4)$$

where the two forcings on the right hand side of the equation are defined in equation (2) for all sky and clear sky, respectively. All the indices have the same meanings as in equation (2). Apparently, this formula can be further rewritten as:

$$NTAIF(x,y,h,t) = \left[\Delta F_{BCRAD}^{allsky}(x,y,h,t) - \Delta F_{BCRAD}^{clearsky}(x,y,h,t)\right] - \left[\Delta F_{REF}^{allsky}(x,y,h,t) - \Delta F_{REF}^{clearsky}(x,y,h,t)\right]. \quad (5)$$

Figure 7. Time evolution of (a) all sky and (b) clear sky radiative forcings (in W/m^2) induced by black carbon aerosols in various OSST and CSST runs; and the latitudinal distributions of (c) clear sky and (d) all sky radiative forcings induced by black carbon aerosols derived from the OSST and SOM runs. The global mean values are derived based on area-weighted averages of the forcings as functions of longitude and latitude for a given vertical layer derived using equation (2). The offline results were derived using the OSST REF run data and equation (3). OSST latitudinal mean data are derived based on the 20-year means. SOM latitudinal mean data are derived based on the last 20-year means.

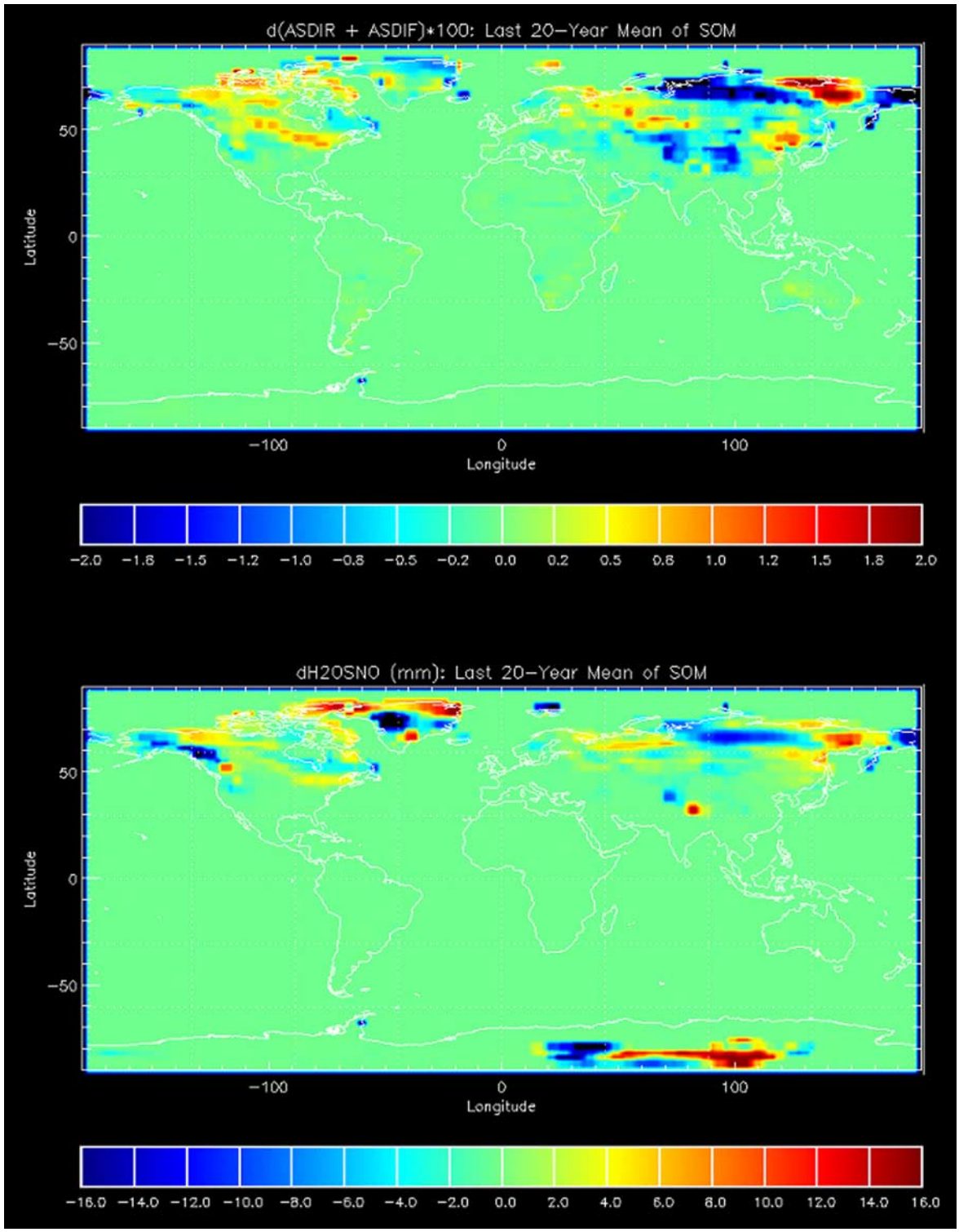

Figure 9. Changes in surface solar albedo (sum of direct and diffusive, or ASDIR + ASDIF, in percent; upper panel) and surface snow depth, or H2OSNO (in mm; lower panel) caused by BC forcing. They are derived by deducting REF run results from BCRAD run results (similar to equation (2)) based on the last 20-year means of SOM run results.

Four terms on the right hand side represent the all-sky and clear-sky forcings in BCRAD and REF runs, respectively. The NTAIF defined in equations (4) or (5) has largely removed the cloud forcing caused by other factors (e.g., sulfate aerosols) under the external mixing assumption. The impact on surface albedo by BC aerosols (a feedback to the forcing rather than a forcing), however, is preserved. The 20-year means of NTAIF derived from OSST model 1 run are -0.07 and -0.05 W/m^2 at the surface and TOA, respectively, or 22% and 11% of the absolute values of the

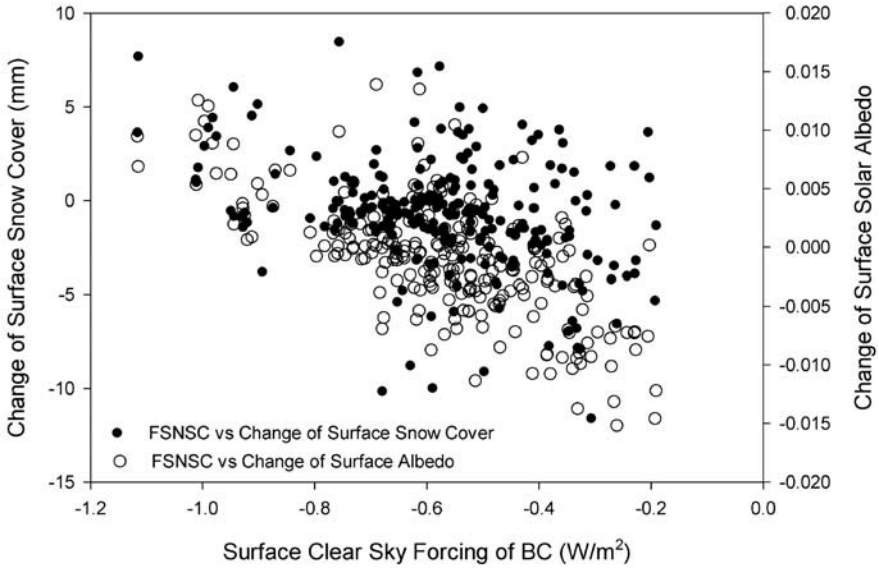

Figure 10. Global-mean of surface clear sky forcing by BC (FSNSC, in W/m^2) versus BC caused changes in northern hemispheric mean of snow depth (in mm) and surface solar albedo. All data are derived based on monthly means of 20-year REF and BCRAD OSST model 1 run results.

corresponding all-sky forcings (Table 5). In contrast, SOM runs predict much larger values of NTAIF than OSST runs (the SOM NTAIF values almost triple the OSST values; see Table 5). This reflects the effect of including the oceanic response to BC forcings in the model. Interestingly, the ranges of variation of annual mean NTAIF during the 20-year integration in OSST runs are very large, namely 0.89 and 0.81 W/m^2 at the TOA and surface, respectively, and this implies a large variability in the thermodynamic kind of BC aerosol-cloud interaction (note the variation range of all-sky forcing is much larger than that of clear-sky forcing; see Table 3). The SOM results with an equilibrium nature exhibit a similar variation range to the OSST results. All integration-means of NTAIF at both TOA and surface from SOM and OSST runs are negative (Table 5), suggesting that in a global-mean and integration-mean base, the effect of NTAIF is to reduce the positive TOA direct forcing while enhance the negative surface direct forcing by BC.

[28] The pattern of longitude-latitude distribution of NTAIF is quite complicated (Figure 12a). Significant NTAIF exists not only over the Northern Hemisphere as expected but also over the southern oceans. The results suggest that changes in atmospheric circulation, especially in the meridional transport of heat and water vapor and thus the vertical air motions, must have been caused by BC forcing (see later discussion). High positive NTAIF can be seen in several places in the high latitudes of the Northern Hemisphere as well as in the southern part of the ITCZ, representing the decreases of cloud cover. The decrease of clouds in polluted areas is apparently due to enhanced evaporation of clouds caused by the warming effect of BC, which is supported by a case study of a marine stratocumulus cloud system off the Indian coast [*Ackerman et al.*, 2000]. When introducing the oceanic feedback to BC forcings in SOM runs, this ''cloud burning'' pattern over several highly polluted areas such as India and eastern China becomes less visible (less positive in terms of NTAIF) than in OSST runs, primarily due to the changes caused in convective cloud cover over the subtropic and tropical regions (Figure 12b, also see later discussion). In SOM runs, BC aerosols cause a substantial change in convective cloud cover and thus a change in NTAIF, representing by a strong negative NTAIF (increase of cloud cover) along the north edge of the ITCZ and a strong positive NTAIF (decrease of cloud cover) in the south part of the ITCZ (Figure 12). At the northern edge of the Eurasian continent, especially over the Russian Far East, a negative forcing induced by a local increase in clouds (mainly low and middle clouds) can be seen. This enhancement of cloud coverage is due to the adiabatic cooling at the surface and in near-surface air caused by a unique distribution of BC aerosols in the middle and upper troposphere over this region as shown in next section. Note that the signature of surface albedo changes (Figure 9) is not quite noticeable in the NTAIF distribution, indicating the effect of this feedback to BC forcings is much smaller than that of the cloud change.

4. Effect of Black Carbon on Climate

4.1. Responses of Surface Properties

[29] The modeled results suggest that BC heats the atmosphere mainly between 5^o and 50^o latitude in the Northern Hemisphere, corresponding to the most polluted areas (Figure 13a). Outside this zone, there are two pairs of heating/cooling areas in the tropics, one in the upper troposphere and one in the lower troposphere, corresponding to the influence of BC caused changes in convective clouds (see later discussion). Note that these two heating/cooling pairs in the tropics are barely visible in the results of OSST and CSST runs. BC caused solar heating applies through

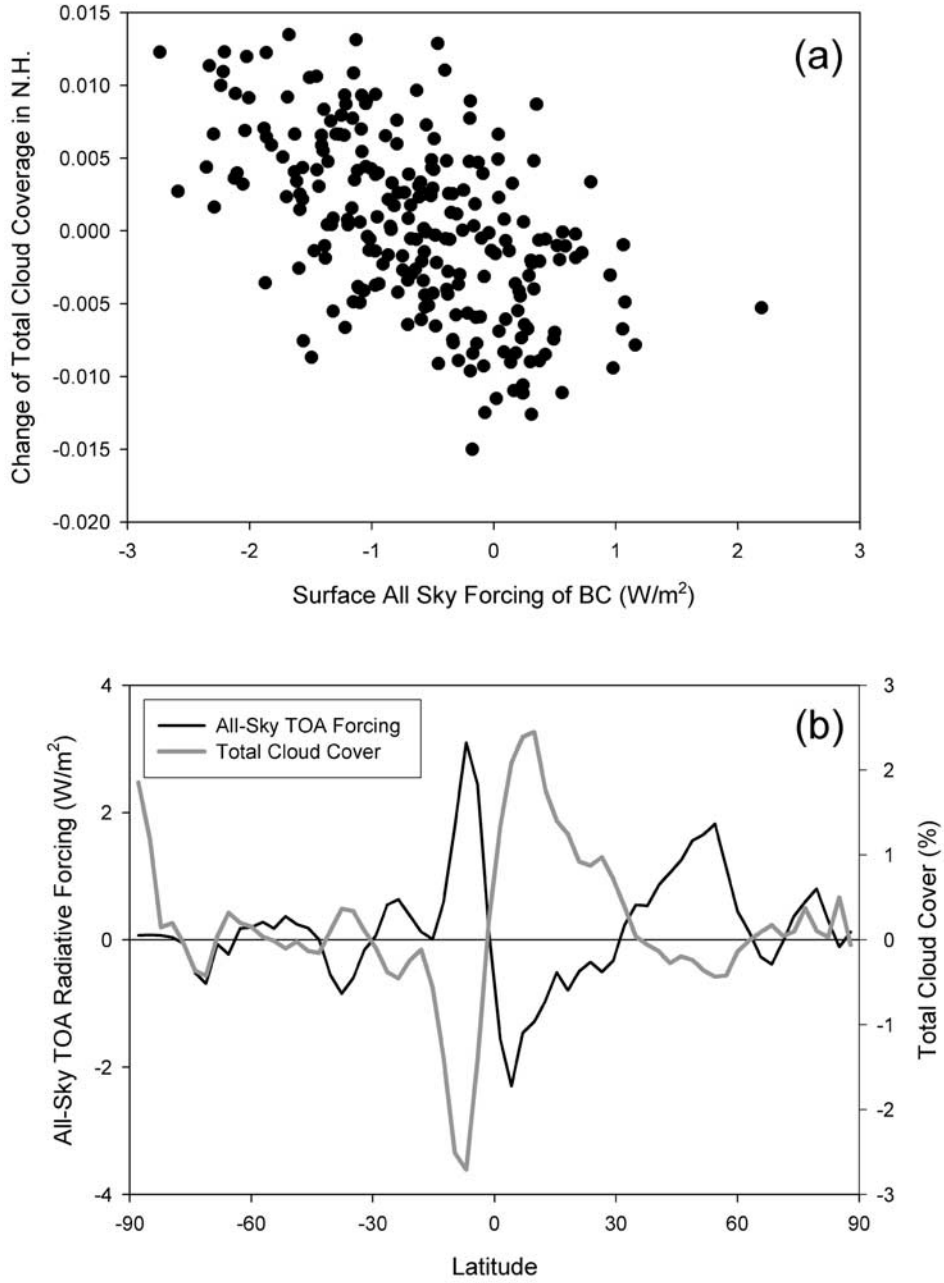

Figure 11. Modeled (a) global-mean all sky forcings of BC at Earth's surface (W/m^2) versus BC caused changes in northern hemispheric mean total cloud covers, where both are monthly means based on 20 years of OSST model 1 run results; and (b) zonal mean changes in total cloud cover (%) versus BC TOA all sky forcings (W/m^2) derived based on the last 20-year means of the SOM run results.

most of the troposphere in the Northern Hemisphere except for the tropics and polar region. At high latitudes in the Northern Hemisphere, BC-induced atmospheric solar heating primarily occurs in the middle and upper troposphere due to horizontal transport of aerosols which most likely were first transported vertically by convection in midlatitudes (interestingly, there is a small cooling zone close to the ground in the high-latitude Northern Hemisphere). Corresponding to the atmospheric heating by BC, there is a significant reduction in absorbed solar radiation by the Earth's surface (Figure 13b) especially in the

Table 5. Annual and Global Mean of NTAIF of BC Presented as Integration Period Mean ± Standard Deviation (Range)[a]

	TOA	Surface
OSST Model 1	−0.05 ± 0.24 (0.81)	−0.07 ± 0.26 (0.89)
OSST Model 2	−0.03 ± 0.23 (1.01)	−0.04 ± 0.25 (1.10)
OSST Model 3	−0.08 ± 0.18 (0.83)	−0.12 ± 0.20 (0.89)
SOM	−0.16 ± 0.31 (1.24)	−0.17 ± 0.34 (1.32)

[a]All in W/m^2. The OSST results are based on the annual means of 20 years; the SOM results are based on the annual means of the last 20 years.

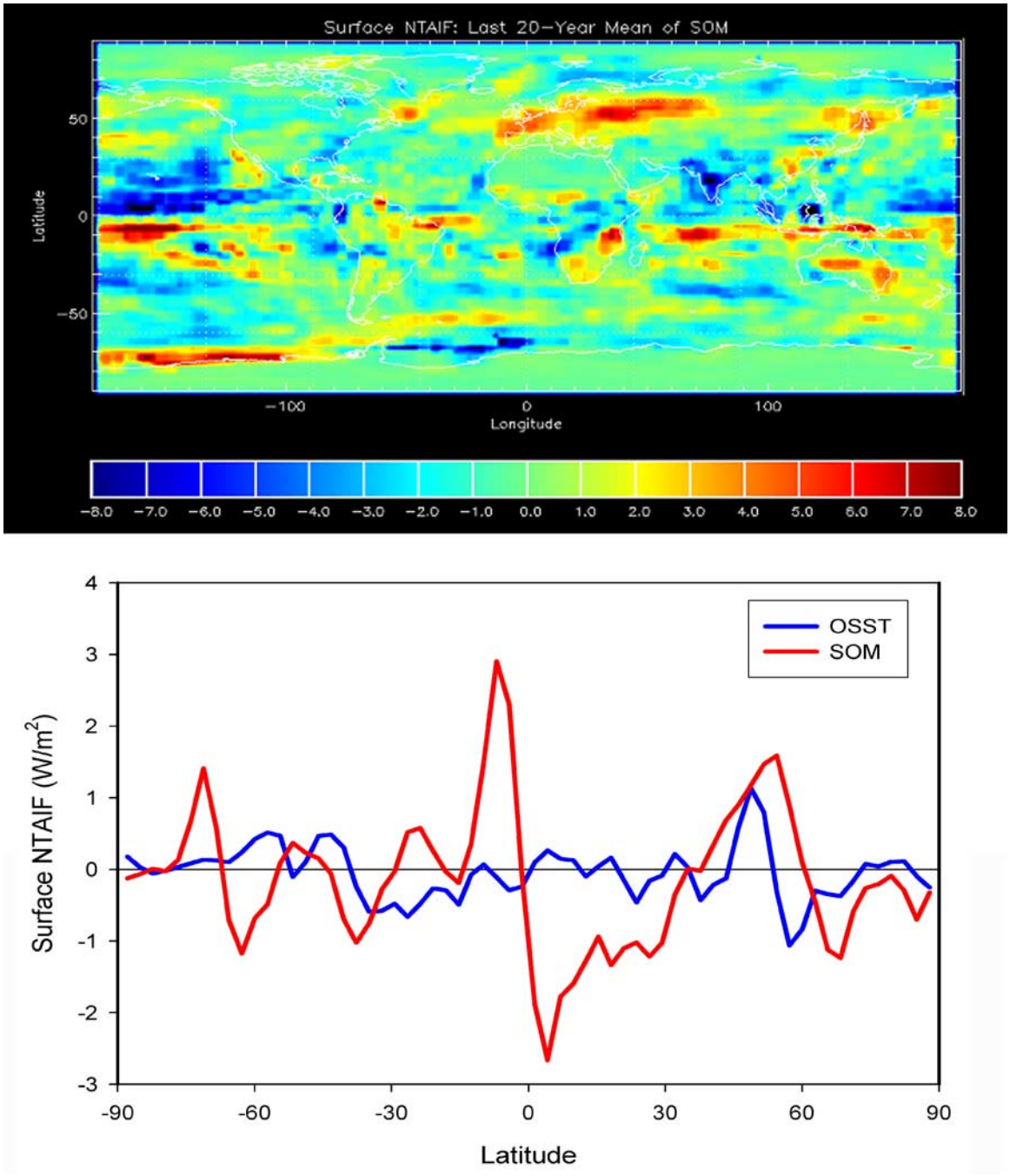

Figure 12. The spatial distribution of the non-Twomey-Albrecht indirect forcing at the surface in W/m^2, derived from the last 20-year means of SOM run using equation (3) (upper panel); and (b) comparison between the zonal means of NTAIF at the surface derived from SOM runs (last 20-year mean) and from OSST runs (20-year mean) (lower panel).

Northern Hemisphere that obviously can lead to a cooling of the ground. This sharp change of the thermodynamic effect caused by BC from warming to cooling across the atmosphere-surface interface generates negative fluxes of both sensible and latent heat in the low and middle latitudes in the Northern Hemisphere to compensate the radiative cooling at the land surface caused by BC aerosols. Resultant changes in land surface temperature are thus determined by the difference between compensating heat fluxes and the reduction in absorbed solar radiation at the surface. The similar processes occur in the atmosphere-ocean surface as shown in SOM runs. Note a previous study using an interactive sulfate aerosol-climate model [*Roeckner et al.*, 1999] has also indicated the similar response of surface heat fluxes to the reduction of incoming solar radiation caused by sulfate aerosols. However, the situation related to BC aerosol becomes more complicated due to BC's atmospheric heating, which is opposite to the sulfate aerosols' cooling effect on atmosphere. In most latitudes of the Northern Hemisphere, negative heat fluxes somewhat offset the cooling

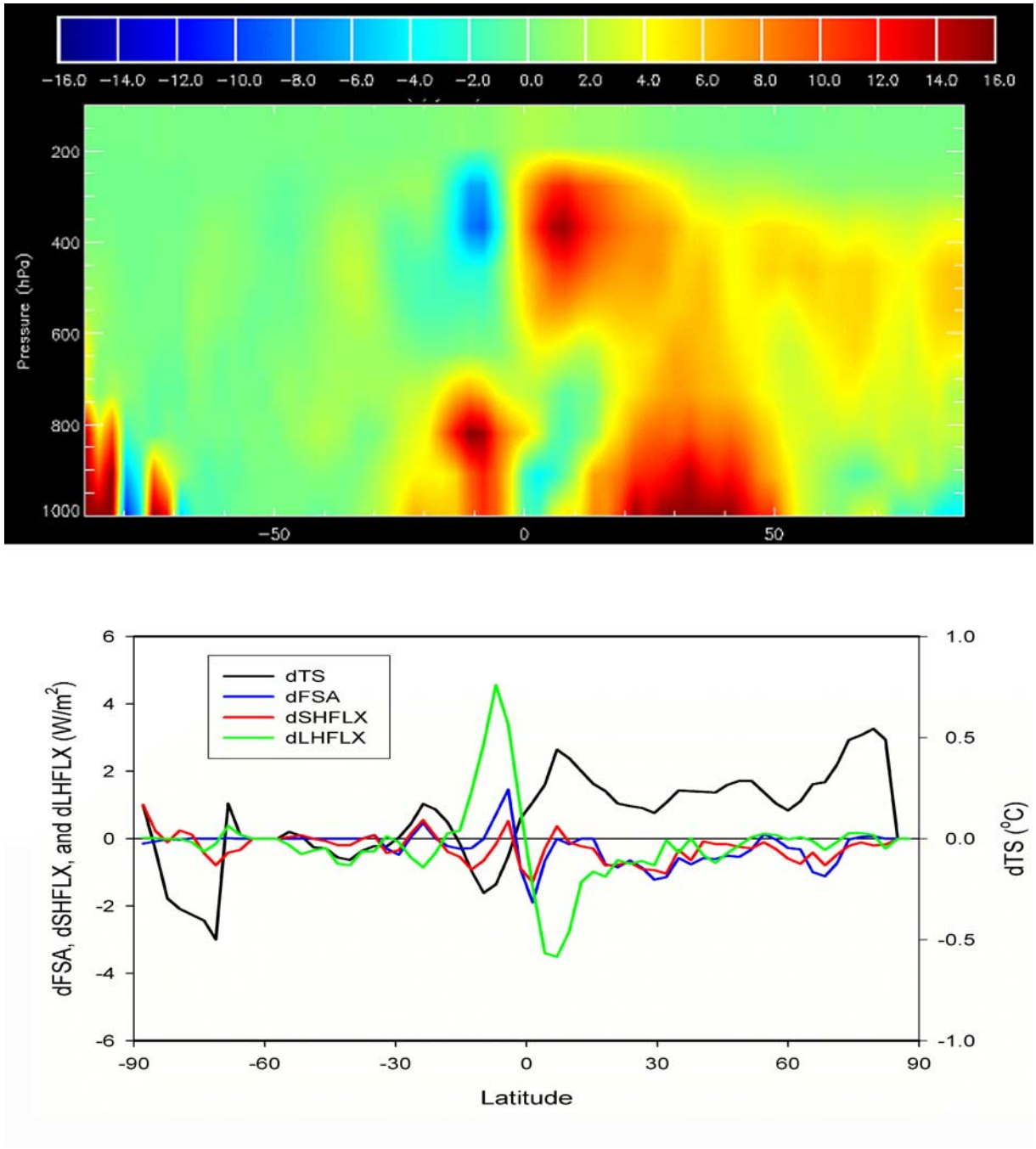

Figure 13. BC caused zonal mean changes of: (a) atmospheric solar heating rate in K/year (upper panel); and (b) solar radiation absorbed by the Earth's land surface (dFSA in W/m^2), latent (dLHFLX) and sensible heat fluxes (dSHFLX; both in W/m^2), and land surface temperature (dTS in °C) (lower panel). All data are the last 20-year averages of SOM run results.

effect caused by the decrease of absorbed solar radiation at the surface. The land surface temperature has slightly increased in these areas. However, in the Southern Hemisphere midlatitudes, the cooling effect caused by reduced surface absorption has not been compensated by the surface heat fluxes and this leads to a decrease of land surface temperature. In the tropics, BC induced cloud effect dominants the surface temperature changes.

[30] The response of surface properties to BC forcings can be also seen from their time evolutions in OSST runs (Figure 14a). The annual means of these variables are found to follow BC radiative forcings closely during the model integration. BC caused changes in net surface long-wave flux and land sensible heat flux were all forced to decrease along time while the land latent heat flux appeared to fluctuate around zero (Figure 14a). It is found that the peak changes in sensible heat flux caused by BC in SOM runs are about twice as large as in OSST runs. Both runs produce the similar latitudinal distributions of above change except in the midlatitude of the Southern Hemisphere (Figure 14b).

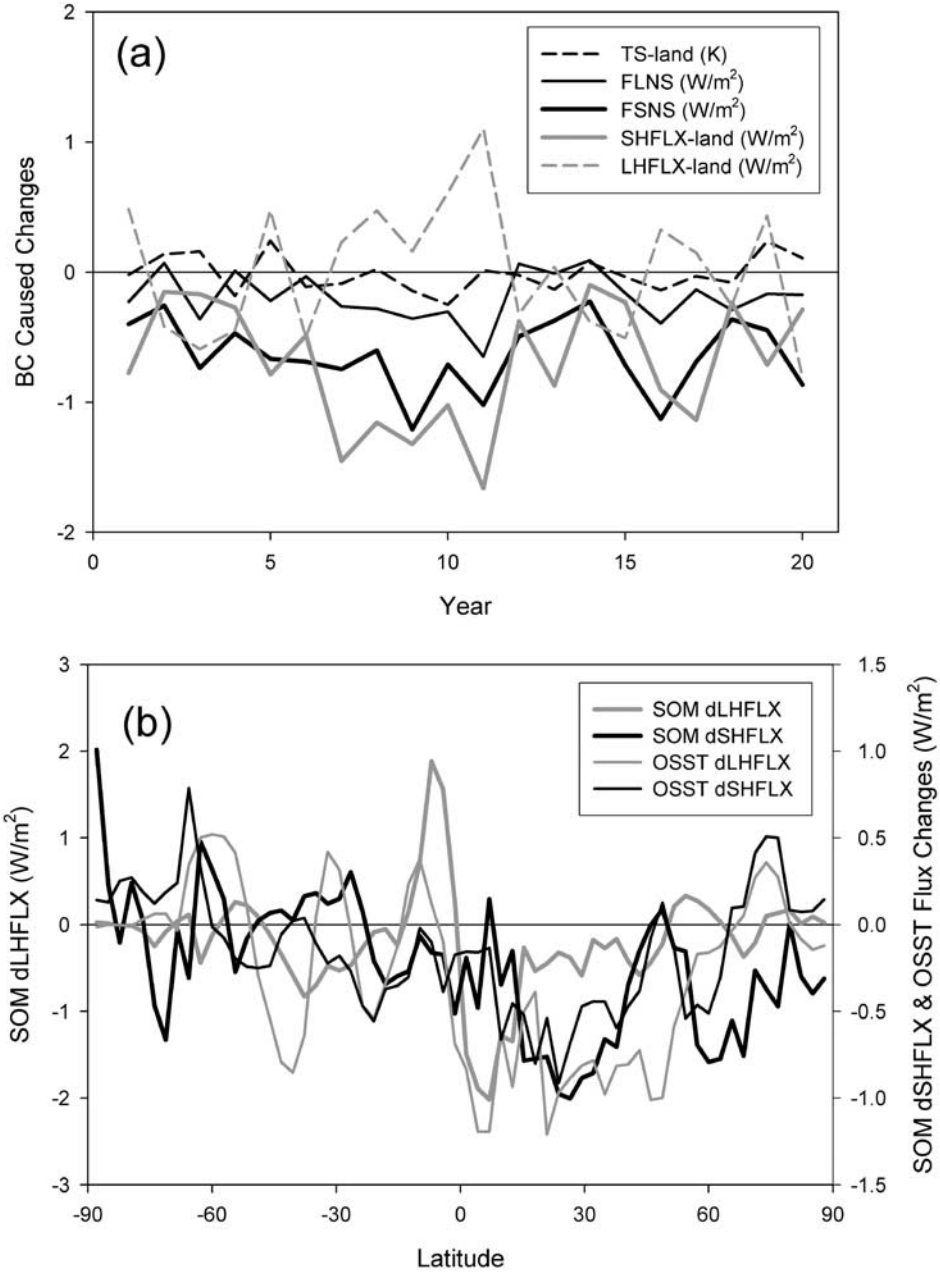

Figure 14. (a) Time evolution of surface all-sky forcing (FSNS, in W/m^2) and BC caused global-mean changes of land surface temperature (TS-land, in °C), net surface long-wave flux (FLNS, in W/m^2), land surface latent heat flux (LHFLX-land, in W/m^2), and land surface sensible heat flux (SHFLX-land, in W/m^2) in the OSST runs (upper panel). (b) Comparison between changes in surface sensible heat flux (dSHFLX) as well as latent heat flux (dLHFLX) between SOM run and OSST run (lower panel; note that here a different scale in vertical axis has been used).

For latent heat flux, the latitudinal distributions predicted by both SOM and OSST runs are similar, the values derived from these two sets of runs, however, differ significantly in several zonal regions including the ones between 20°N and 40°N (note that a different axis for the changes in SOM latent heat flux in the figure is used) in the higher latitude of the Northern Hemisphere and in a large portion of the Southern Hemisphere. This indicates that the differing oceanic responses included in these two sets of runs lead to a difference in oceanic evaporation (Figure 14b). Negative changes in latent and sensible heat fluxes exist in most latitudinal zones showing a strong compensation to the surface cooling caused by BC. In both OSST and SOM runs, the global and annual mean height of planetary boundary layer (PBL) has been lowered by more than 2 m due to the effect of BC radiative forcings on the surface energy budget (Tables 6 and 7). This change largely exceeds the natural variability of the height of PBL.

[31] There is no monotonic warming or cooling "trend" that can be derived from the modeled annual mean surface

Table 6. BC Caused Changes of Selected Parameters in Comparison With Their Reference Standard Deviations Derived Based on 20 Years of Results of the OSST Model Runs[a]

	Reference Standard Deviation σr	Model 1 Mean ± σ (range)	Model 2 Mean ± σ (range)	Model 3 Mean ± σ (range)
Ts, °C	0.11	−0.01 ± 0.04 (0.13)	0.00 ± 0.05 (0.21)	0.00 ± 0.05 (0.20)
Ts-land, °C	0.16	−0.01 ± 0.14 (0.49)	−0.00 ± 0.15 (0.66)	0.00 ± 0.12 (0.43)
FLNS, W/m^2	0.32	−0.19 ± 0.19 (0.74)	−0.32 ± 0.18 (0.65)	−0.30 ± 0.20 (0.79)
SHFLX, W/m^2	0.16	−0.26 ± 0.15 (0.55)	−0.35 ± 0.14 (0.51)	−0.36 ± 0.13 (0.43)
SHFLX-land, W/m^2	0.38	−0.71 ± 0.48 (1.56)	−0.65 ± 0.46 (2.06)	−0.96 ± 0.43 (1.32)
LHFLX, W/m^2	0.47	−0.39 ± 0.24 (0.94)	−0.41 ± 0.19 (0.84)	−0.42 ± 0.24 (0.88)
LHFLX-land, W/m^2	0.34	0.01 ± 0.50 (1.91)	−0.06 ± 0.46 (2.01)	−0.08 ± 0.49 (1.83)
ASDIFR, × 100	0.20	−0.02 ± 0.23 (0.06)	−0.01 ± 0.06 (0.20)	−0.01 ± 0.20 (0.04)
CLDHGH, %	0.30	−0.00 ± 0.21 (0.84)	−0.06 ± 0.20 (0.72)	−0.04 ± 0.17 (0.77)
CLDMED, %	0.12	−0.07 ± 0.15 (0.56)	−0.08 ± 0.10 (0.41)	−0.08 ± 0.11 (0.37)
CLDLOW, %	0.14	0.14 ± 0.12 (0.45)	0.21 ± 0.15 (0.59)	0.18 ± 0.11 (0.39)
PRECC, mm/year	4.93	−5.74 ± 3.19 (11.4)	−5.89 ± 2.41 (9.27)	−5.52 ± 3.30 (12.8)
PRECL, mm/year	2.05	0.79 ± 1.74 (6.10)	0.78 ± 1.45 (5.77)	0.31 ± 2.08 (7.19)
PBLH, m	1.37	−2.13 ± 1.11 (4.33)	−2.99 ± 1.58 (5.77)	−3.12 ± 1.78 (7.56)

[a]Note: Here Ts = surface temperature, FLNS = net surface long-wave flux, SHFLX = surface sensible heat flux, LHFLX = surface latent heat flux, ASDIFR = land surface diffusive and direct albedo of solar radiation, CLDHGH = high cloud cover, CLDMED = middle cloud cover, CLDLOW = low cloud cover, PRECC = convective precipitation rate, PRECL = large-scale precipitation rate, and PBLH = height of planetary boundary layer; σ represents the standard deviation of changes, range = maximum − minimum.

temperature change caused by BC during the 20-year integration period of OSST runs using all three different sets of optical parameters (Figure 15a). Under the radiative forcing by BC aerosols, the forced change of surface temperature experiences a short warming period (year 2–5) then a long but slight cooling period (year 6–18; note Model 3 showed a weak warming trend at year 8, 11, and 14) and finally swings upward again in the last two years. It is worthwhile to note that the changes in annual mean surface temperature caused by BC in many years during the model integration are clearly smaller than the reference standard deviation, i.e., the modeled natural variability (see also Table 6). The 20-year means of BC caused change in surface temperature produced by OSST model 1 run is −0.01°C or practically zero.

[32] The annual mean change in surface temperature caused by BC derived from SOM runs shows a variation between −0.1 and +0.3°C (Figure 15b). The 5-year running average curve in the last ∼20 year defines equilibrium with a mean value of +0.09°C, slightly higher than the modeled nature variability of 0.07°C (Figure 15b and Table 7). With a limited heat capacity of the ocean, SOM runs perhaps represent the upper limit of the system response to BC forcings. Therefore it cannot be concluded that black carbon will cause a significant global-scale change in the Earth's surface temperature based on the results of this study.

[33] However, in the regional scale, BC can cause significant changes in surface temperature over several locations, including a warming across most part of the Eurasian Continent and coolings over eastern China, most part of North America, South America, and several places in central Africa (not shown), all exceeding or close to the natural variability of land surface temperature in these places.

4.2. Response of Atmospheric Circulation and Cloud Cover

[34] It has been found that introducing BC radiative effect in the model has clearly altered the meridional sensible and latent heat transport, convective fluxes, in particular over the tropics, and thus the atmospheric circulation (Figure 16). Deep convection in the north part of the ITCZ has been clearly enhanced due to the existence of BC, while the strength of convection in the south part of the ITCZ is substantially reduced. The resultant cloud cover change over tropics closely follows the change in convection. The latitudinal distributions of meridional transport of heat in BCRAD runs have also been modified compared with the results of REF run, corresponding to the changes in convective fluxes. The most substantial change in meridional heat transport is a significantly enhanced northward flux across the equator in the lower troposphere and an enhanced southward transport in the upper troposphere over the same latitudes. This change in meridional heat transport is initiated by the enhancement of convection in the north side of ITCZ, mainly caused by increased atmospheric instability due to BC aerosols from highly polluted regions (Figure 16; also Figures 2 and 6). The change in meridional heat transport then in turn enhances convection in the north part of the ITCZ while weakens convection in the south part so that both the annual-mean and seasonal-mean convection centers of the ITCZ has actually been shifted or modified.

Table 7. BC Caused Changes of Selected Parameters in Comparison With Their Reference Standard Deviations Derived Based on the Last 20 Years of Results of the SOM Model Runs

	Reference Standard Deviation σr	Last 20 Years Mean ± σ (range)
Ts, °C	0.07	0.09 ± 0.07 (0.23)
Ts-land, °C	0.14	0.16 ± 0.17 (0.59)
FLNS, W/m^2	0.23	−0.31 ± 0.34 (1.16)
SHFLX, W/m^2	0.12	−0.27 ± 0.17 (0.57)
SHFLX-land, W/m^2	0.44	−0.46 ± 0.58 (2.44)
LHFLX, W/m^2	0.22	−0.26 ± 0.34 (1.38)
LHFLX-land, W/m^2	0.52	−0.32 ± 0.63 (2.11)
ASDIFR, ×100	0.12	−0.02 ± 0.05 (0.17)
CLDHGH, %	0.40	0.11 ± 0.32 (1.15)
CLDMED, %	0.12	−0.04 ± 0.16 (0.61)
CLDLOW, %	0.12	0.15 ± 0.22 (0.78)
PRECC, mm/year	2.72	−3.58 ± 3.93 (14.8)
PRECL, mm/year	1.57	0.29 ± 2.39 (9.56)
PBLH, m	1.86	−2.47 ± 2.56 (9.41)

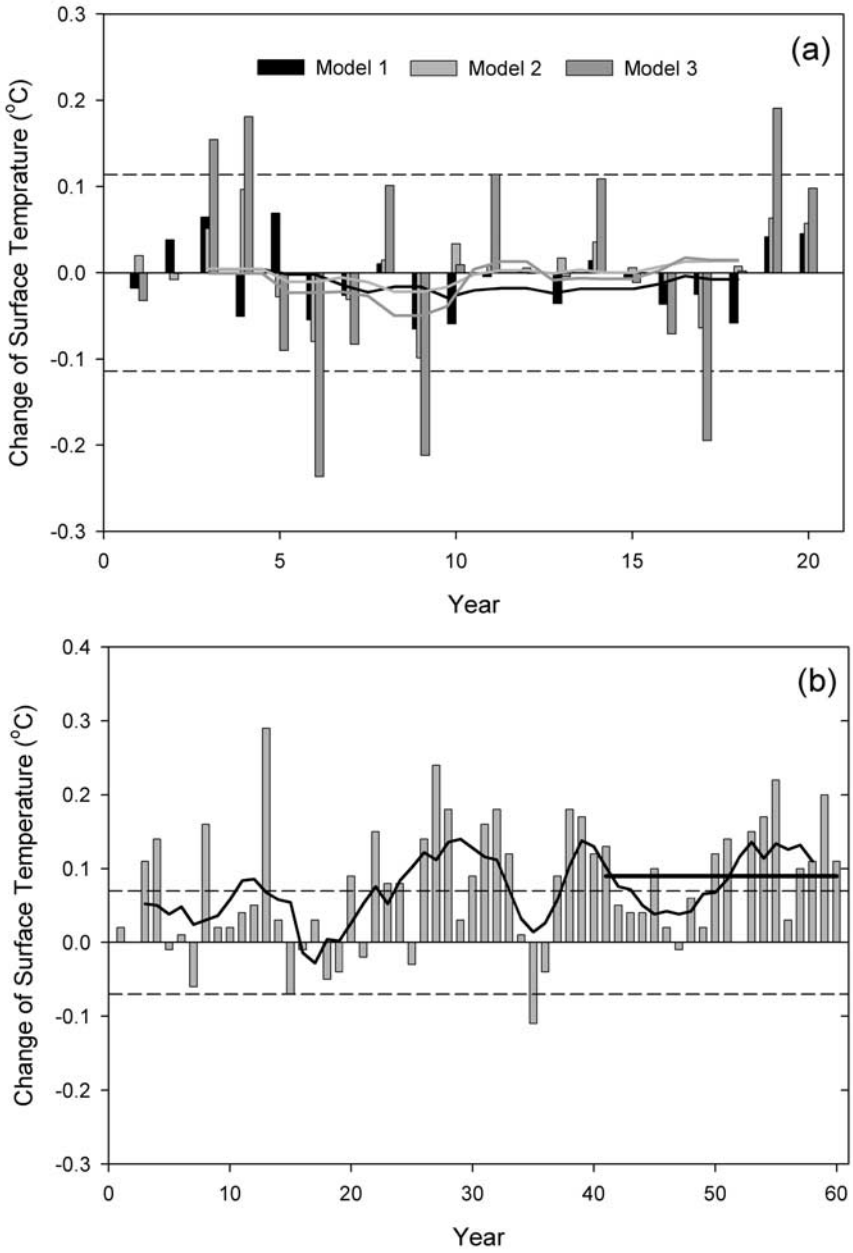

Figure 15. Forced changes of annual and global mean surface temperature by black carbon aerosols in (a) OSST 20 year runs (upper panel) and (b) SOM 60 year runs (lower panel); each is derived by subtracting the temperatures of the REF run from corresponding BCRAD runs. The solid lines show the 5-year running averages, the dotted lines show the reference standard deviations, and the thick solid line in the lower panel shows the last-20-year mean. Global mean values are area-weighted averages.

This positive feedback between convection and meridional heat transport due to BC forcing has also been revealed by *Chung et al.* [2002] and *Menon et al.* [2002] in studies on the climate effect of absorbing aerosols over India and China. Besides the changes in the tropics, convection and associated cloud cover in the middle latitude of the Northern Hemisphere from ~40 to 50°N are reduced. In the high latitudes of the Northern Hemisphere, cloud cover is increased without any clear connection to convection as discussed in previous section.

[35] The global and integration means of changes in high and middle cloud covers are not significant compared to their natural variability while the change in low cloud cover is slightly higher than its modeled natural variability (Tables 6 and 7). However, the numbers of global means of high and middle clouds might be misleading because the modeled changes of these two types of clouds due to BC forcings often have opposite signs across the equator and can offset each other in the global mean calculation (Figure 16a). Low cloud cover in OSST runs was slightly increased throughout most period of the integration due to BC caused cooling in the lower troposphere, while the high and middle cloud covers both experienced an increase (mainly in the first 8 years) and then decrease during the

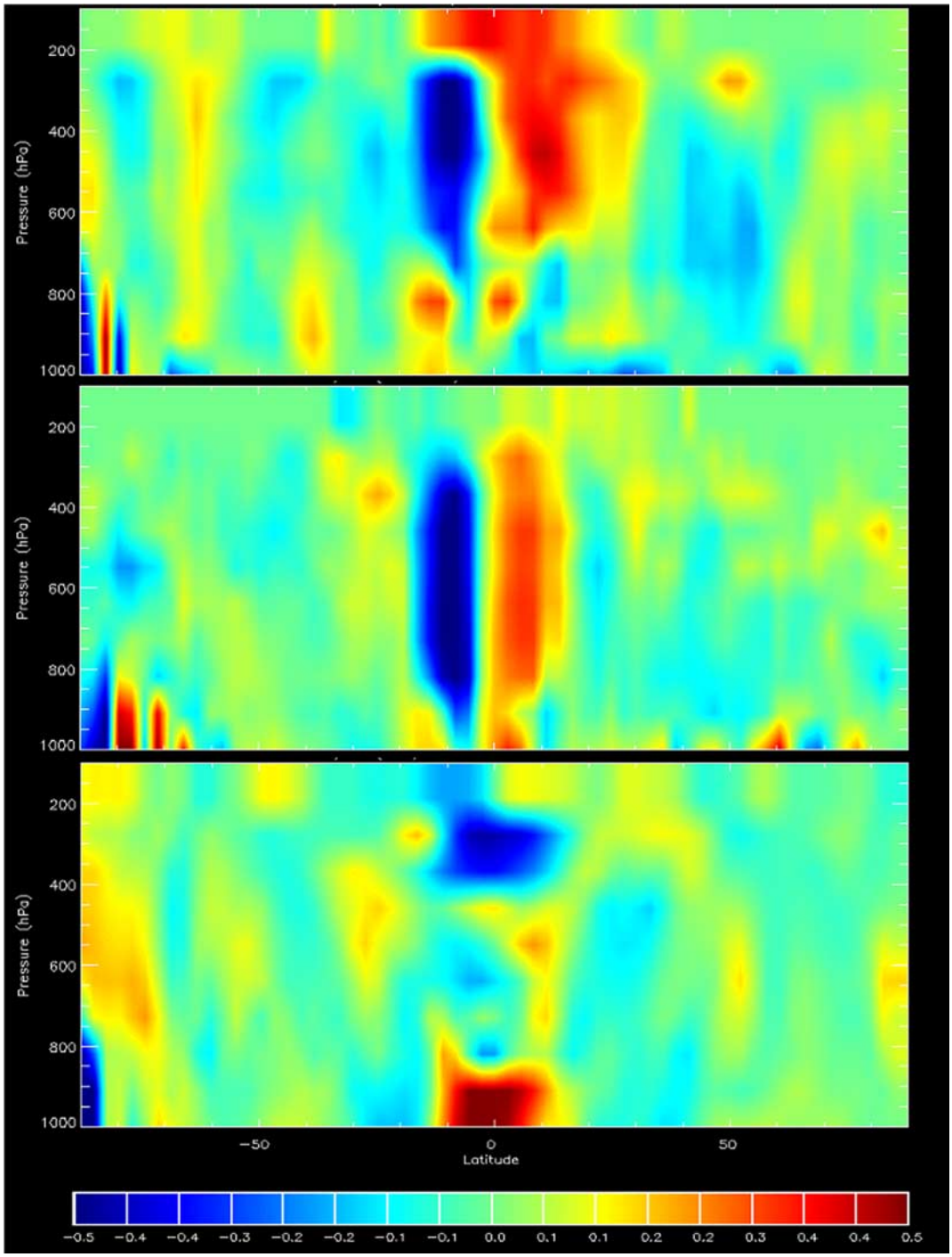

Figure 16. Ratios of BC caused changes to the standard deviations of these changes (note: not the reference standard deviation) derived based on the monthly data of (a) total cloud fraction (top panel), (b) total moist convective fluxes (middle panel), and (c) meridional transport of sensible heat (lower panel). Results are zonal means based on the last 20-year averages from SOM runs. The moisture flux is positive upward, and the meridional flux is positive northward.

20-year model integration. SOM runs provide a different latitudinal distribution of cloud cover than OSST runs, particularly between 15°S and 30°N (Figure 17a), due to the different response of convection and thus atmospheric circulations to BC forcings as previously discussed. Outside the tropical and subtropical zones, the SOM results are close to the OSST results. Note that the modeled global and integration mean of high cloud cover has different signs in SOM runs than in OSST runs (Tables 6 and 7).

4.3. Response of Precipitation

[36] It has been found that BC forcings lead to a significant decrease of convective precipitation rate in both SOM and OSST runs. In fact, the change in convective precipi-

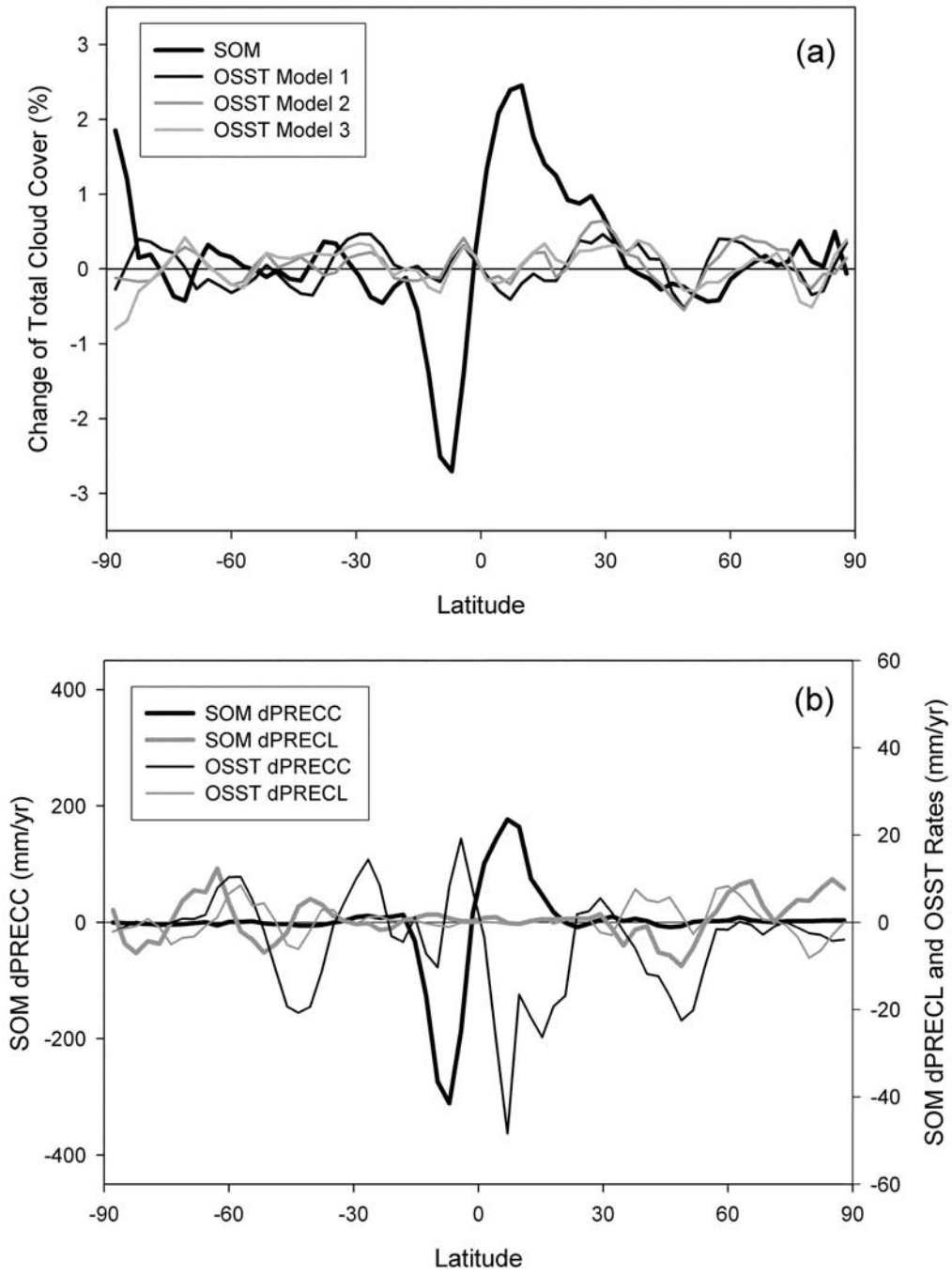

Figure 17. Comparison of modeled latitudinal changes caused by BC between SOM and OSST runs in (a) total cloud cover (in percentage, upper panel); and (b) precipitation rates (in mm/year). SOM run results are the last 20-year means and OSST run results are 20-year integration means.

tation rate is among the most substantial climate effect of BC aerosols found in this study (Tables 6 and 7). In OSST runs, the change of convective precipitation rate caused by BC is consistently on the negative side along the model integration, while the change in large-scale precipitation rate varied around the zero. The global mean value of BC caused change in convective precipitation does not reflect the significant changes in several latitudinal zones (Figures 17b and 18a). In addition, the largest zonal mean change in convective precipitation rate in SOM runs is about 8 times as large as that in OSST runs (Figure 17b; note the different vertical axes are used in this figure), concentrated in the tropics. Opposite to the results of convective precipitation, the latitudinal distributions of changes in large-scale precipitation rate predicted by both sets of model runs are quite close to each other.

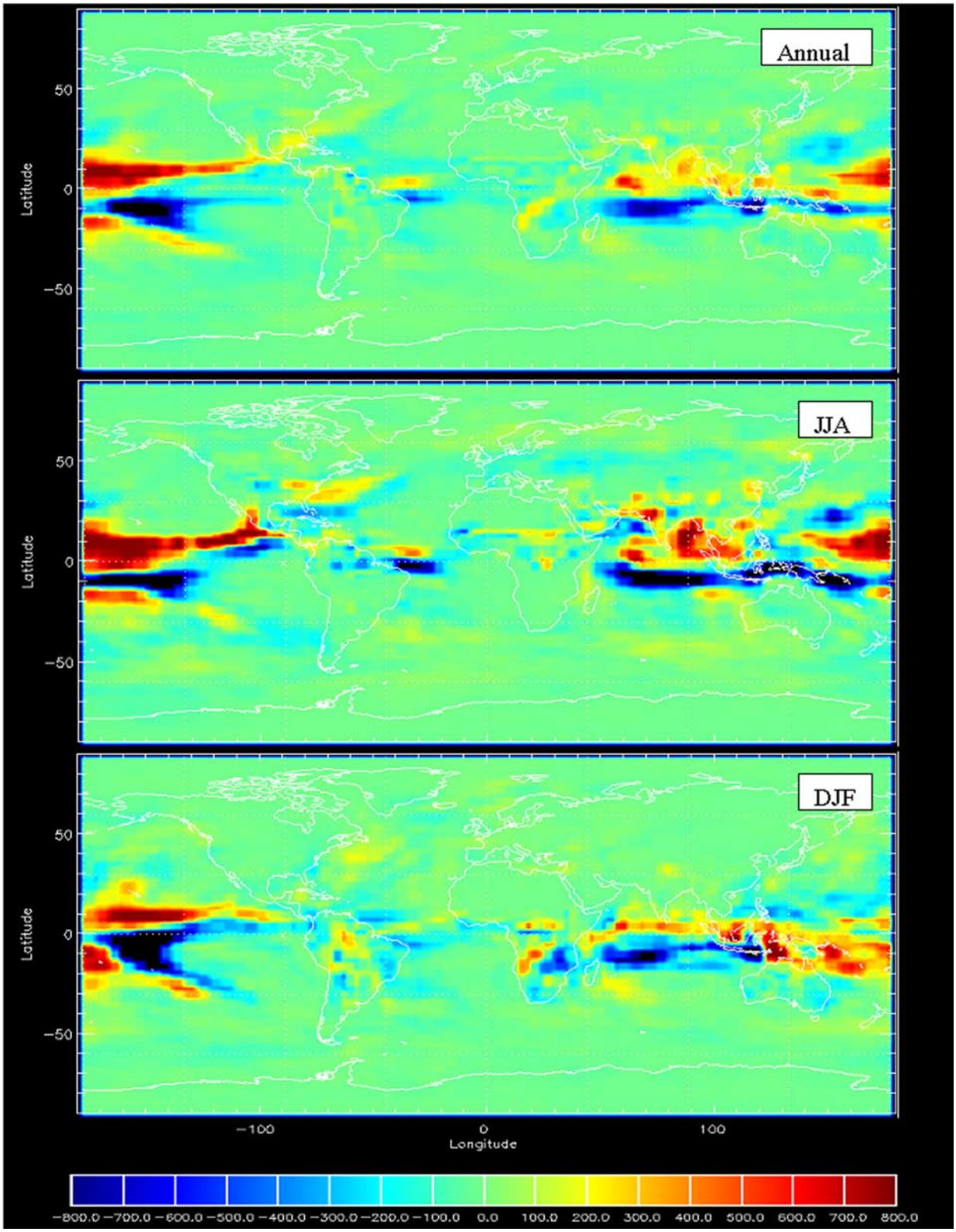

Figure 18. Modeled (a) annual mean (upper panel), (b) June–July–August mean (middle panel), and (c) December–January–February mean (lower panel) of changes in convective precipitation rate (mm/year) caused by BC. Data are derived using the last 20-year means of SOM runs.

[37] During the period of June–July–August (hereafter JJA), BC caused enhancement in convective precipitation rate mainly occurs in the north part of the ITCZ, across the central Pacific as well as over a large portion of the northern Indian Ocean (Figure 18b). The maximum zonal-mean enhancement is about 15% compared with the rate in REF run. This zone of enhancement in precipitation is accompanied by a narrow (latitudinal) band just south to it with a significantly reduced convective precipitation rate (as large as 23% reduction to the REF run result in a zonal-mean base). These two zones approximately separated by the equator and the northward meridional transport of heat between these two zones has been substantially enhanced (see also discussion in the previous section). In the central South Pacific, a second zone of precipitation enhancement appears along a not well-defined South Pacific Convergence Zone (SPCZ) [*Vincent*, 1994], primarily due to dynamic reason. In the period of December–January–February (hereafter DJF), BC caused enhancement in convective precipitation rate becomes weaker than in JJA (Figure 18c). The distribution of regions with enhanced precipitation rate is also different than that in JJA, expanded along the northwest to southeast direction and from the east coast of Africa, across the Indian Ocean, to the South Pacific. The east part of this band is apparently distributed along the SPCZ, which is much better defined during the Northern Hemisphere winter than summer and clearly influenced by not only dynamics but also the aerosols transported largely from southeast Asia, Australia, and perhaps South Asia. The maximum zonal-mean enhancement of convective precipitation cause by BC during the months of DJF is about 7% in the north part of the ITCZ. The largest reduction of precipitation in the south part of the ITCZ during the same period is about 6%. Interestingly, the similar pattern of changes in convective precipitation over the Indian subcontinent and the north Indian Ocean was also found by *Chung et al.* [2002] using the CCM3 model with a climatological SST data set and a prescribed aerosol forcing profile of the observed haze layer over above region.

[38] Concentrated heavy precipitation bands in the tropics traditionally define the ITCZ, which normally consist of a north and a south band separated by the equator in a zonal-mean base (except in the months of March–April–May). The relative precipitation strength of the north band in comparison with the south one is different in different seasons. The finding in this study of the enhancement of convective activity along with precipitation in the northern portion and the reduction of these quantities in the southern portion of the ITCZ induced by BC forcings suggests that the location of the most concentrated zones of precipitation and convective activity in the tropics can be switched or modified due to the impact of BC aerosols.

5. Discussion and Conclusion

[39] This article has presented a three-dimensional interactive BC aerosol-climate model and the results of several sets of relatively long numerical simulations using this model, driven by a 20-year-long monthly dataset of observed SST, a repeated 12-month climatological SST data, or by a slab ocean model, all using a constant annual emission of BC (14 TgC/year).

[40] It has been demonstrated that the actual radiative forcings of BC derived using the interactive model exhibit significant interannual variations related to the changes in cloud cover and surface albedo, all caused by BC forcings themselves. Under the influence of the indirect effects and responses or feedbacks to BC direct forcings, the interactive model runs provide smaller positive all-sky forcings at the TOA and larger negative all-sky forcings at the surface than the offline diagnostics (the direct forcings). With an absolute amount 2 times higher than that of the TOA forcing, the surface forcing by BC, which directly induces significant changes to various climate parameters, is an important factor in analyzing the climate impact of BC. Results from this study and many previous ones [see *Haywood and Boucher*, 2000; *Penner et al.*, 2001; *Ramaswamy et al.*, 2001; *Ramanathan et al.*, 2001a, 2001b; *Chung et al.*, 2002] challenge the practice of using only the TOA radiative forcing by BC to project the possible climate impact of BC.

[41] The radiative forcings of BC cause many changes to the climate system including the circulation of the atmosphere. As the results have demonstrated, responses of the modeled climate to BC aerosol radiative forcings are complicated, and in many occasions and locations the resultant changes in the atmosphere or at the Earth's surface compensate each other.

[42] Among the most significant regional changes caused by BC revealed in this study is the change in precipitation rate and pattern. This ''redistribution of precipitation'' is represented by the shift of precipitation centers in the tropics and subtropical regions (mainly along the ITCZ and SPCZ) as well as by the change in snow depth in the middle and high latitudes of the Northern Hemisphere. Convection and associated precipitation are found to be substantially enhanced (as much as 15% in zonal-mean precipitation rate) in the north portion of the ITCZ and south portion of the SPCZ, while they are significantly reduced (up to 23% in zonal-mean precipitation rate) in the south part of the ITCZ and the north part of the SPCZ. BC effect also causes many changes in meridional heat transport including an enhanced northward flux in the lower troposphere and an enhanced southward flux in the upper troposphere across the ITCZ. Snow depth over many high or even midlatitude regions in the Northern Hemisphere is found to be changed by $\sim\pm$20% and the surface albedo in these regions thus has been modified.

[43] When compared with the model's natural variability, the most significant global-scale changes caused by BC aerosols occurred in surface latent heat flux, surface net long-wave flux, height of planetary boundary layer, convective precipitation rate, surface sensible heat flux, and the cover of low clouds (Figure 19, Tables 6 and 7), all related to the hydrological cycle or near-surface heat budget and are results of either direct forcing by BC at the surface or the modified atmospheric circulation by BC. It is worth noting that the actual changes of several parameters in certain latitudes are much larger in absolute values than their global means.

[44] It is important to indicate that the results of both OSST and SOM model runs with an annual BC emissions of $\sim$14 TgC (note that similar numbers have been used in several related studies) do not suggest a significant

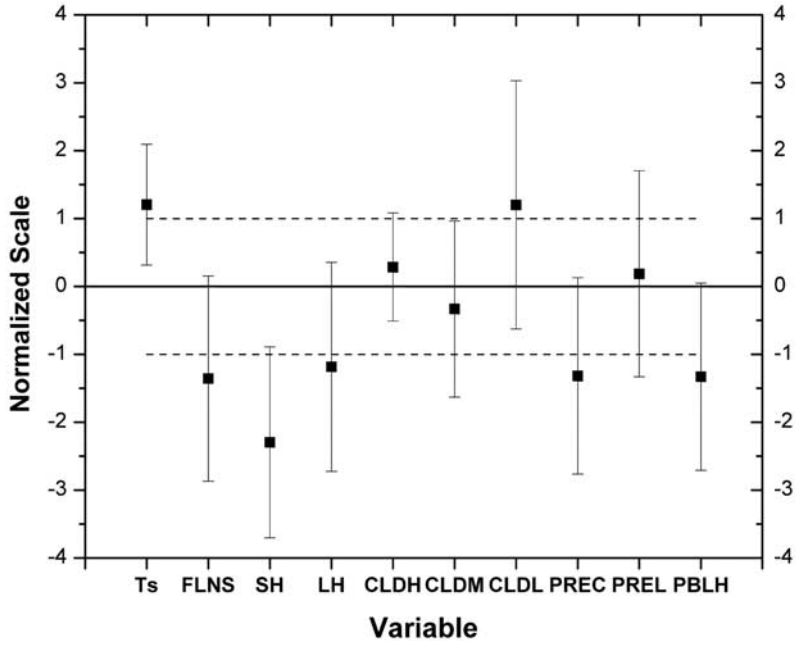

Figure 19. The means and standard deviations of BC caused changes of selected model variables normalized using the corresponding reference standard deviations. Here Ts = surface air temperature, FLNS = net long-wave flux at the surface, SH = surface sensible heat flux, LH = surface latent heat flux, CLDH = high cloud cover, CLDM = middle cloud cover, CLDL = low cloud cover, PREC = convective precipitation rate, PREL = large-scale precipitation rate, and PBLH = height of PBL. Two dash lines mark the range of standard deviation of the REF run (normalized to be 1). Black squares label the means and two bars extended from the mean represent the range of standard deviation of the change. The results are from the last 20 years of SOM runs.

change in global mean surface temperature attributed to BC forcings (note in particular that the SOM run results represent the upper bound of the system response to BC forcings). This is because the calculated surface temperature change is determined by a subtle balance among changes in surface energy budget as well as changes in the hydrological cycle, all caused by BC radiative forcing. Although BC caused changes in hydrological cycle or near-surface heat budget are quite significant, the combined effect of them on the global-mean surface temperature appears to be small. It is worth noting that there are clear (some are significant) differences between results using OSST or SOM model. A good example is the BC caused changes in convection and convective precipitation rate in the tropics.

[45] The results of this study show that the influences of BC aerosols on climate and environment are more significant in regional scale than in global scale. The regional climate effects of BC are represented by persistent reduction or enhancement of convection and cloud cover in certain regions, as well as by altered precipitation rate and snow depth then surface albedo. The changes in cloud cover caused by BC forms a "non-Twomey-Albrecht" indirect forcing. This NTAIF, in a global-mean base, tends to weaken the positive BC solar forcing at the top of the atmosphere while enhances the negative BC forcing at the Earth's surface. This study indicates several important feedbacks between BC radiative effects and climate dynamics. In particular, BC caused changes in surface albedo and in cloud cover are responsible for the significant interannual variations of BC's clear-sky and all-sky radiative forcings, respectively, and thus lead to significantly modified actual forcings by BC compared to BC's direct forcings. This suggests the importance of using interactive aerosol-climate models to address the issues related to the climate impacts of aerosols.

[46] It is of course true that current descriptions of many above-mentioned processes even in the most sophisticated climate models still have room for improvement. In particular, simulations of aerosol behaviors in the GCMs like the ones in this study are quite crude in some aspects, especially those related to aerosol size-dependent processes or dealing with microphysical conversions. This suggests a great uncertainty in estimating possible changes in climate, especially in cloud processes and surface temperature, caused by black carbon aerosols. A detailed analysis on this issue clearly requires further improvement in the representations of aerosol size distributions as well as mixing status in the model. In addition, high-resolution mesoscale models with more detailed physics and chemistry are needed to enhance our knowledge of the climate effects of absorbing aerosols and to provide possible improvements of climate models.

[47] A major simplification made in this study, i.e., assuming external mixing states of black carbon aerosols, could influence the final results quantitatively. This assumption could potentially lead to an underestimate of the forcing strength of BC [*Chýlek et al.*, 1995; *Fuller et al.*, 1999]. However, this simplification should not qualitatively change the major conclusions other than enhancing them. Additionally, the slab ocean model cannot accurately represent the transient response of the atmosphere-ocean system to BC radiative forcings, though the equilibrium results provided

by this type of models can help us to understand the upper limit of climate impact of BC aerosols. Future studies using coupled atmosphere-ocean models and more comprehensive aerosol modules will improve several shortcomings of this study.

[48] **Acknowledgments.** This study was supported by the industrial consortium of the MIT Joint Program on the Science and Policy of Global Change, by DOE grants DE-FGO2-94ER61937 and DE-FGO2-93ER61713, and by the US EPA under the Cooperative Agreement XA-83042801-0. The author thanks M. Mayer for helping to derive the BC emissions and F.-M. Bréon and S. Generoso for providing POLDER aerosol index data. He also thanks R. Prinn, J. Kiehl, P. Rasch, W. Collins, A. Sokolov, C. Forest, and P. Stone for discussions and suggestions. Two anonymous reviewers provided many constructive suggestions that significantly improved the manuscript. The Climate and Global Dynamics Division (CGD) of NCAR has provided computer codes, related datasets, and excellent technique support for the CCM3 and LSM.

References

Ackerman, A. S., O. B. Toon, D. E. Stevens, A. J. Heymsfield, V. Ramanathan, and E. J. Welton (2000), Reduction of tropical cloudiness by soot, *Science*, *288*, 1042–1047.

Albrecht, B. A. (1989), Aerosols, cloud microphysics, and fractional cloudiness, *Science*, *245*, 1227–1230.

Babiker, M., et al. (2001), The MIT Emissions Prediction and Policy Analysis (EPPA) Model: Revisions, sensitivities, and comparison of results, *Rep. 71*, MIT Joint Program on the Science and Policy of Global Change, Cambridge, Mass. (Available at http://web.mit.edu/globalchange/www/MITJPSPGC_Rpt71.pdf).

Bodhaine, B. A. (1995), Aerosol absorption measurements at Barrow, Mauna Loa and the south pole, *J. Geophys. Res.*, *100*, 8967–8975.

Bohren, C. F., and D. R. Huffman (1983), *Absorption and Scattering of Light by Small Particles*, 530 pp., John Wiley, New York.

Bonan, G. B. (1998), The land surface climatology of the NCAR Land Surface Model coupled to the NCAR Community Climate Model, *J. Clim.*, *11*, 1307–1326.

Boville, B. A., and P. R. Gent (1998), The NCAR Climate System Model, version one, *J. Clim.*, *11*, 1115–1130.

Bréon, F.-M., D. Tanré, and S. Generoso (2002), Aerosol effect on cloud droplet size monitored from satellite, *Science*, *295*, 834–838.

Briegleb, B. P. (1992), Delta-Eddington approximation for solar radiation in the NCAR Community Climate Model, *J. Geophys. Res.*, *97*, 7603–7612.

Chung, C. E., V. Ramanatahn, and J. T. Kiehl (2002), Effects of the South Asian absorbing haze on the northeast monsoon and surface-air heat exchange, *J. Clim.*, *15*, 2462–2476.

Chung, S. H., and J. H. Seinfeld (2002), Global distribution and climate forcing of carbonaceous aerosols, *J. Geophys. Res.*, *107*(D19), 4407, doi:10.1029/2001JD001397.

Chýlek, P., G. Videen, D. Ngo, R. G. Pinnick, and J. D. Klett (1995), Effect of black carbon on the optical properties and climate forcing of sulfate aerosols, *J. Geophys. Res.*, *100*, 16,325–16,332.

Cooke, W. F., and J. J. N. Wilson (1996), A global black carbon aerosol model, *J. Geophys. Res.*, *101*, 19,395–19,409.

Cooke, W. F., C. Liousse, H. Cachier, and J. Feichter (1999), Construction of a $1^\circ \times 1^\circ$ fossil fuel emission data set for carbonaceous aerosol and implementation and radiative impact in the ECHAM4 model, *J. Geophys. Res.*, *104*, 22,137–22,162.

Cooke, W. F., V. Ramaswamy, and P. Kasibhatla (2002), A general circulation model study of the global carbonaceous aerosol distribution, *J. Geophys. Res.*, *107*(D16), 4279, doi:10.1029/2001JD001274.

Crutzen, P. J., and M. O. Andreae (1990), Biomass burning in the tropics: Impact on atmospheric chemistry and biogeochemical cycles, *Science*, *250*, 1669–1678.

Flossmann, A. I., W. D. Hall, and H. R. Pruppacher (1985), A theoretical study of wet-removal of atmospheric pollutants, I. The redistribution of aerosol particles captured through nucleation and impaction scavenging by growing cloud drops, *J. Atmos. Sci.*, *42*, 582–606.

Fuller, K. A., W. C. Malm, and S. M. Kreidenweis (1999), Effect of mixing on extinction by carbonaceous particles, *J. Geophys. Res.*, *104*, 15,941–15,954.

Hansen, J., M. Sato, and R. Ruedy (1997), Radiative forcing and climate response, *J. Geophys. Res.*, *102*, 6831–6864.

Hansen, J., M. Sato, R. Ruedy, A. Lacis, and V. Oinas (1998), Global warming in the twenty-first century: An alternative scenario, *Proc. Natl. Acad. Sci. USA*, *97*, 9875–9880.

Haywood, J. M., and O. Boucher (2000), Estimates of the direct and indirect radiative forcing due to tropospheric aerosols: A review, *Rev. Geophys.*, *38*, 513–543.

Haywood, J. M., and V. Ramaswamy (1998), Global sensitivity studies of the direct radiative forcing due to anthropogenic sulfate and black carbon aerosols, *J. Geophys. Res.*, *103*, 6043–6058.

Haywood, J. M., and K. P. Shine (1995), The effect of anthropogenic sulfate and soot aerosol on the clear sky planetary radiation budget, *Geophys. Res. Lett.*, *22*, 603–606.

Haywood, J. M., D. L. Roberts, A. Slingo, J. M. Edwards, and K. P. Shine (1997), General circulation model calculations of the direct radiative forcing by anthropogenic sulphate and fossil-fuel soot aerosols, *J. Clim.*, *10*, 1562–1577.

Houghton, J. T., et al. (Eds.) (1996), *Climate Change 1995: The Science of Climate Change*, 572 pp., Cambridge Univ. Press, New York.

Jacobson, M. (2001), Strong radiative heating due to the mixing state of black carbon in atmospheric aerosols, *Nature*, *409*, 695–697.

Jennings, S. G., and R. G. Pinnick (1980), Relationships between visible extinction, absorption and mass concentration of carbonaceous smokes, *Atmos. Environ.*, *14*, 1123–1129.

Kiehl, J. T., and B. P. Briegleb (1993), The relative roles of sulfate aerosols and greenhouse gases in climate forcing, *Science*, *260*, 311–314.

Kiehl, J. T., J. J. Hack, G. B. Bonan, B. A. Boville, B. L. Briegleb, D. L. Williams, and P. J. Rasch (1996), Description of the NCAR Community Climate Model (CCM3), *Tech. Note TN-420 + STR*, Climate and Global Dynamics Div., Natl. Cent. for Atmos. Res., Boulder, Colo. (Available at http://www.cgd.ucar.edu/cms/ccm3/TN-420).

Kiehl, J. T., J. J. Hack, G. B. Bonan, B. A. Boville, D. L. Williams, and P. J. Rasch (1998), The National Center for Atmospheric Research Community Climate Model: CCM3, *J. Clim.*, *11*, 1131–1149.

Koch, D. (2001), The transport and direct radiative forcing of carbonaceous and sulfate aerosols in the GISS GCM, *J. Geophys. Res.*, *106*, 20,311–20,332.

Li, Y. (1996), Global population distribution database, *Sub-Project FP/1205-95-12*, United Nations Environ. Progr., Paris.

Liousse, C., J. E. Penner, C. Chuang, J. J. Walton, H. Eddleman, and H. Cachier (1996), A global three-dimensional model study of carbonaceous aerosols, *J. Geophys. Res.*, *101*, 19,411–19,432.

Lohmann, U., and J. Feichter (2001), Can the direct and semi-direct aerosol effect compete with the indirect effect on a global scale?, *Geophys. Res. Lett.*, *28*, 159–161.

Manabe, S., and R. T. Wetherald (1967), Thermal equilibrium of the atmosphere with a given distribution of relative humidity, *J. Atmos. Sci.*, *24*, 241–259.

Mayer, M., R. Hyman, J. Harnisch, and J. Reilly (2000), Emissions inventories and time trends for greenhouse gases and other pollutants, *Tech. Note 1*, 49 pp., MIT Joint Program on the Science and Policy of Global Change, Cambridge, Mass.

Menon, S., J. Hansen, L. Nazarenko, and Y. Luo (2002), Climate effects of black carbon aerosols in China and India, *Science*, *297*, 2250–2253.

Myhre, G., F. Stordal, K. Restad, and I. Isaksen (1998), Estimates of the direct radiative forcing due to sulfate and soot aerosols, *Tellus, Ser. B*, *50*, 463–477.

Olivier, J. G. J., et al. (1995), Description of EDGAR Version 2.0, *Rep. 771060002*, Natl. Inst. of Public Health and the Environ., Bilthoven, Netherlands.

Penner, J. E., C. C. Chuang, and K. Grant (1998), Climate forcing by carbonaceous and sulfate aerosols, *Clim. Dyn.*, *14*, 839–851.

Penner, J. E., et al. (2001), Aerosols, their direct and indirect effects, in *Climate Change 2001: The Scientific Basis*, edited by J. T. Houghton et al., Cambridge University Press, New York.

Prinn, R. G., et al. (1999), Integrated global system model for climate policy analysis: I. Model framework and sensitivity studies, *Clim. Change*, *41*, 469–546.

Pruppacher, H. R., and J. D. Klett (1997), *Microphysics of Clouds and Precipitation*, 2nd ed., Kluwer Acad., Norwell, Mass.

Ramanathan, V., P. J. Crutzen, J. T. Kiehl, and D. Rosenfeld (2001a), Aerosol, climate, and the hydrological cycle, *Science*, *294*, 2119–2124.

Ramanathan, V., et al. (2001b), Indian Ocean Experiment: An integrated analysis of the climate forcing and effects of the great Indo-Asian haze, *J. Geophys. Res.*, *106*, 28,371–28,398.

Ramaswamy, V., et al. (2001), Radiative forcing of climate change, in *Climate Change 2001: The Scientific Basis*, edited by J. T. Houghton et al., Cambridge Univ. Press, New York.

Roeckner, E., L. Bengtsson, J. Feichter, J. Lelieveld, and H. Rodhe (1999), Transient climate change simulations with a coupled atmosphere-ocean GCM including the tropospheric sulfur cycle, *J. Clim.*, *12*, 3004–3032.

Satheesh, S. K., and V. Ramanathan (2000), Large differences in tropical aerosol forcing at the top of the atmosphere and Earth's surface, *Nature*, *405*, 60–63.

Streets, D. G., S. Gupta, S. T. Waldhoff, M. Q. Wang, T. C. Bond, and B. Yiyun (2001), Black carbon emissions in China, *Atmos. Environ.*, *35*, 4281–4296.

Tegen, I., D. Koch, A. A. Lacis, and M. Sato (2000), Trends in tropospheric aerosol loads and corresponding impact on direct radiative forcing between 1950 and 1990: A model study, *J. Geophys. Res.*, *105*, 26,971–26,989.

Twitty, J. T., and J. A. Weinman (1971), Radiative properties of carbonaceous aerosols, *J. Atmos. Sci.*, *10*, 725–731.

Twomey, S. (1977a), *Atmospheric Aerosols*, 302 pp., Elsevier Sci., New York.

Twomey, S. (1977b), The influence of pollution on the shortwave albedo of clouds, *J. Atmos. Sci.*, *34*, 1149–1152.

Vincent, D. G. (1994), The South Pacific Convergence Zone: A review, *Mon. Weather Rev.*, *122*, 1949–1970.

Wang, C., and J. S. Chang (1993), A three-dimensional numerical model of cloud dynamics, microphysics, and chemistry: 1. Concepts and formulation, *J. Geophys. Res.*, *98*, 14,827–14,844.

Wang, C., and R. G. Prinn (2000), On the roles of deep convective clouds in tropospheric chemistry, *J. Geophys. Res.*, *105*, 22,269–22,297.

Wilson, J., C. Cuvelier, and F. Raes (2001), A modeling study of global mixed aerosol fields, *J. Geophys. Res.*, *106*, 34,081–34,108.

C. Wang, Massachusetts Institute of Technology, Room E40-425, Cambridge, MA 02139-4307, USA. (wangc@mit.edu)